

Activation of Somatostatin Inhibitory Neurons by Lypd6-nAChRa2 System Restores Juvenile-like Plasticity in Adult Visual Cortex

Masato Sadahiro¹⁻⁵†, Michael P. Demars¹⁻⁵†, Poromendro Burman¹⁻⁵, Priscilla Yevoo¹⁻⁵, Milo R. Smith¹⁻⁵, Andreas Zimmer⁶, Hirofumi Morishita^{1-5*}

¹ Department of Psychiatry, ² Department of Neuroscience, ³ Department of Ophthalmology, ⁴ Mindich Child Health and Development Institute, ⁵ Friedman Brain Institute, Icahn School of Medicine at Mount Sinai, New York, NY 10029, USA

⁶ Institute of Molecular Psychiatry, Medical Faculty, University of Bonn, Bonn 53127, Germany

*Contact to: hirofumi.morishita@mssm.edu

† M.S. and M.P.D. share co-first authorship

Abstract

Heightened juvenile cortical plasticity declines into adulthood, posing a challenge for functional recovery following brain injury or disease. A network of inhibition is critical for regulating plasticity in adulthood, yet contributions of specific interneurons other than parvalbumin (PV) interneurons have been underexplored. Here we show Lypd6, an endogenous positive modulator of nicotinic acetylcholine receptors (nAChRs), as a specific molecular target in somatostatin (SST) interneurons to reactivate cortical plasticity in adulthood. Selective overexpression of Lypd6 in adult SST interneurons reactivates plasticity through $\alpha 2$ subtype of nAChR by rapidly activating SST interneurons which in turn inhibit PV interneurons, a key early trigger of the juvenile form of plasticity. Chemogenetic activation of SST interneurons confirmed the causal role of SST interneuron activity in reactivating plasticity. Identification of Lypd6-nAChR $\alpha 2$ system and associated SST-PV disinhibitory circuits as the first SST interneuron-specific targets for reactivation of plasticity in adulthood provides potential therapeutic insights into treating disorders with limited recovery due to diminished plasticity such as amblyopia as well as psychiatric disorders characterized by deficits in SST interneurons.

39 Introduction

40 Experience-dependent brain plasticity is heightened during juvenile critical periods but this
 41 declines into adulthood, which poses a major challenge to functional recovery following injury or
 42 disease later in life ^{1,2}. A prevailing concept of therapeutic strategy to support restoration of function
 43 from such enduring debilitating conditions is to reactivate juvenile-like levels of heightened plasticity in
 44 the adult brain. One of the best-studied models of critical period plasticity is ocular dominance plasticity
 45 – the enduring loss of responsiveness in primary visual cortex (V1) to an eye deprived of vision ³ that
 46 results in amblyopia, a disorder of sight that affects 2–4% of the human population and has limited cure
 47 in adulthood. This model has long served to not only understand the fundamental regulatory
 48 mechanisms of critical periods, but also importantly to facilitate the discovery of novel targets to achieve
 49 reactivation of visual plasticity in adulthood.

50 Over the past decade, with the advent of gene targeting in mice ⁴⁻⁷, the network of cortical
 51 inhibition was elucidated as one of the critical mechanisms for regulation of visual plasticity. The
 52 developmental initiation of the critical period can be accelerated or delayed by genetically or
 53 pharmacologically altering GABAergic inhibition in visual cortex ⁸⁻¹⁶. Following critical period closure in
 54 the adult cortex, plasticity can be induced through pharmacological suppression of GABA_A receptors ¹⁷
 55 or through the transplantation of GABAergic precursors derived from the medial ganglionic eminence
 56 (MGE) ¹⁸⁻²⁰. To date, the role of GABAergic signaling in cortical plasticity has largely focused on
 57 parvalbumin (PV) interneurons ^{15,18,21-23}, where a number of known molecular mediators of plasticity
 58 appear to converge including orthodenticle homeobox protein 2 (otx2) ^{15,24} and perineuronal nets ²³. A
 59 recent report has shown that PV interneuron activity was reduced during the initial 24 hours following
 60 visual deprivation only during the juvenile critical period but not in adulthood. Mimicking this early
 61 reduction in firing using chemogenetic means in adult animals led to reactivation of plasticity,
 62 suggesting that PV interneuronal activity may be instructive for plasticity in visual cortex ²². While their
 63 importance for plasticity in the visual cortex is undeniable, PV interneurons represent only one member

of a diverse group of cortical GABAergic interneurons²⁵. The role of other subclasses of GABAergic interneurons, such as those expressing the peptide somatostatin (SST) that represent nearly a third of the cortical GABAergic interneurons, had largely been ignored until recently^{19,26}. The molecular and circuit mechanisms underlying SST interneuron-mediated regulation of cortical plasticity remain completely unknown.

SST interneurons are promising targets for reactivating plasticity in the adult brain, as they are ideally situated to integrate multiple inputs including bottom-up sensory signals²⁷, and neuromodulation²⁸ induced by locomotion²⁹⁻³³, or by top-down regulation³⁴⁻³⁶. Moreover, SST interneurons highly innervate local PV interneurons, which places them in an ideal position to drive the rapid inhibition instructive to the juvenile form of plasticity. The neuromodulation of SST interneurons by nicotinic signaling that occurs in several brain regions^{28,37-39}, may represent one potential means of restoring plasticity in the adult brain. Our previous study showed that an endogenous inhibitor of nicotinic Acetylcholine Receptors (nAChRs), Lynx1, is enriched in PV interneurons and actively limits V1 plasticity following the critical period⁴⁰. The Lynx family of proteins are GPI-anchored membrane proteins and have a unique toxin-like protein structure, which enables them to bind to the extracellular face of nAChRs expressed in the same cells and regulate their signaling⁴¹. Our recent study further showed that another closely related member of the Lynx family, Lypd6, is enriched in SST interneurons in V1⁴². Interestingly, Lypd6 has been shown to potentiate calcium currents through nicotinic receptors⁴³ in direct contrast to the action of Lynx1⁴⁴. Here we sought to elucidate the potential for nicotinic modulation by Lypd6 in SST interneurons in the regulation of ocular dominance plasticity. This work provides the first molecular mechanism specifically associated with SST interneurons to reactivate plasticity in adult visual cortex.

Results

Neuronal overexpression of Lypd6 prolongs ocular dominance plasticity into adulthood.

First, to examine the expression profile of *Lypd6* in adult V1 where plasticity is limited versus that of juvenile critical period with heightened plasticity, we performed *in situ* hybridization to label *Lypd6* mRNA in V1 of mice at P28 (critical period) and >P60 (adult). We found that *Lypd6* expression is significantly lower in the adult compared to juvenile period which inversely correlates with the extent of ocular dominance plasticity (Fig. 1a, 1b: $*P=0.02$, Student's *t*-test). While *Lypd6* expression was even higher at P18 (pre-critical period) (p18: 244.91 \pm 19.28 normalized to p60 data in Fig. 1a, $p<0.05$ vs P28 or adult), interpretation of *Lypd6* contribution to nicotinic signaling during the pre-critical period is confounded by various additional developmental changes that could impact nicotinic signaling beyond *Lypd6* (e.g. nAChRs, cholinergic projections)⁴⁵.

Based on this decline in *Lypd6* expression in adult V1, we tested if overexpression of *Lypd6* in adulthood could prolong ocular dominance plasticity beyond the critical period, utilizing a transgenic mouse line with pan neuronal overexpression of *Lypd6* (*Lypd6Tg*)⁴³. Following a 4-day short-term monocular deprivation (4d MD) (Fig. 1c), ocular dominance plasticity was assessed in anesthetized mice using a 16-channel linear silicone probe⁴⁶. Each recorded V1 cell was assigned an ocular dominance (OD) score based on the relative balance of strengths of visually evoked responses of the cell to the visual stimulus independently presented to the contralateral and ipsilateral eye. Adult (>P60) *Lypd6Tg* mice that underwent 4d MD show a significant shift in eye preference (OD shift) in V1, away from the deprived contralateral eye and towards the non-deprived ipsilateral eye, compared to non-deprived (no MD) adult *Lypd6Tg* mice or adult wild type (WT) mice that typically display no significant levels of plasticity regardless of visual deprivation (Fig. 1d: *Lypd6Tg* 4d MD vs. WT 4d MD: $****P<0.0001$, vs. *Lypd6Tg* no MD: $****P<0.0001$, *Lypd6Tg* no MD vs. WT no MD: $P=0.28$, χ^2 test). Cumulative distributions of ocular dominance index (ODI: -1=most ipsilateral dominant, 0=equal/binocular, 1=most contralateral dominant) for each recorded cell from each cohort show a significantly higher percentage of single neuronal responses that are relatively ipsilateral dominant in the *Lypd6Tg* 4d MD mice compared to control groups (Fig. 1e: vs. WT 4d MD: $****P<0.0001$, vs.

Lypd6Tg no MD: $***P=0.0002$, Lypd6Tg no MD vs. WT no MD: $P=0.2332$, Kolmogorov-Smirnov (K-S) test). Lastly, individual animal level comparisons of contralateral bias index (CBI) scores – the relative strength to which the visually evoked activity of V1 neurons from the contralateral eye dominates over that from the ipsilateral eye, show a significant decrease only in the Lypd6Tg 4d MD mice (Fig 1f: $****P<0.0001$, one-way analysis of variance (ANOVA). Lypd6Tg 4d MD significantly differs from all other groups: WT no MD, WT4d MD, and Lypd6Tg no MD: respectively, $****P<0.0001$, $**P=0.0023$, and $*P=0.0208$; Tukey's multiple comparisons test). Altogether the results suggest that Lypd6 is a novel positive regulator of ocular dominance plasticity.

Lypd6 expression specifically in SST interneurons reactivates ocular dominance plasticity in adult V1.

While the prior experiments outline the sufficiency of neuronal overexpression of Lypd6 for prolonging ocular dominance plasticity into adulthood, the transgenic line does not provide temporal, spatial, or cell-type information regarding this modulation. In order to address these questions, we developed a Cre-dependent AAV vector for Lypd6 overexpression (AAV8-DIO-EGFP-2A-Lypd6: AAV-Lypd6) (Fig. 2a). Our previous study established that Lypd6 is most highly expressed in SST interneurons in V1 with lower expression in a subset of glutamatergic neurons⁴². Therefore, we characterized Lypd6 overexpression in V1 SST interneurons through viral injection of AAV-Lypd6 into adult SST-cre mice or in V1 glutamatergic neurons through dual viral injection of AAV-Lypd6 combined with an AAV with a cre expression vector driven by a CamKII promoter (AAV8-CamKIIa-mCherry-Cre: AAV-CamKII-cre) into adult WT mice similar to previous reports^{29,47}. The viral injections were adjusted to target the deep cortical layers, comparable to the area where the endogenous expression of Lypd6 has been previously reported to be localized⁴². In both conditions the GFP expression was restricted to SST or glutamatergic populations and provided robust overexpression of Lypd6 in V1 (Fig. 2b, c, d: $****P<0.0001$, Student's *t*-test; and Supplementary Fig. 1).

Next, we assessed the ability of SST or glutamatergic overexpression of Lypd6 in V1 of adult animals to induce ocular dominance plasticity. We injected AAV-Lypd6 or control AAV vector (AAV8-hSyn-DIO-EGFP: AAV-GFP) into adult SST-cre mice and, after >3 weeks of viral incorporation, subjected them to 4d MD (Fig. 2e). In adult mice with SST-specific Lypd6 overexpression that underwent 4d MD (SST-Lypd6 4d MD), there was a significant OD shift compared to non-deprived (no MD) counterparts (SST-Lypd6 no MD) or control 4dMD mice with AAV-GFP injected (SST-GFP 4d MD) (Fig. 2f: SST-Lypd6 4d MD vs. CamKII-Lypd6 4d MD: **** $P < 0.0001$, vs. SST-Lypd6 no MD: **** $P < 0.0001$, vs. SST-GFP 4d MD: *** $P = 0.0006$, χ^2 test). To test whether glutamatergic overexpression of Lypd6 would also induce plasticity in adult mice, we injected a viral cocktail of AAV-CamKII-cre with either AAV-Lypd6 or AAV-GFP into V1 of adult WT mice and, after >3 weeks, subjected them to 4d MD (Fig. 2e). The viral cocktail approach resulted in 93.2% of cells successfully co-transfected (GFP-positive) with AAV-DIO-GFP-Lypd6 and AAV-CamKII-Cre as positive for the excitatory cell marker vGlut1 (Supplemental Fig 1c.), and 52.2% of total vGlut1-positive population as GFP-positive (Supplemental Fig. 1d). We did not observe significant shift in OD in mice with glutamatergic overexpression of Lypd6 that underwent 4d MD (CamKII-Lypd6 4d MD) or control counterparts (CamKII-Lypd6 no MD and CamKII-GFP 4dMD) (Fig. 2f: CamKII-Lypd6 4d MD vs. CamKII-GFP 4d MD: $P = 0.67$, χ^2 test). The cumulative distributions of ODI also show only a significant shift in the SST-Lypd6 4d MD mice (Fig. 2g: SST-Lypd6 4d MD vs. CamKII-Lypd6 4d MD: **** $P < 0.0001$, vs. SST-Lypd6 no MD: *** $P = 0.0001$, vs. SST-GFP 4d MD: *** $P = 0.0002$. CamKII-Lypd6 4d MD vs. CamKII-GFP 4d MD: $P = 0.49$, K-S test). Lastly, comparisons of CBI scores show a significant decrease only in the SST-Lypd6 4d MD mice (Fig. 2h: ** $P = 0.0012$, one-way ANOVA. SST-Lypd6 4d MD significantly differs from: SST-Lypd6 no MD, SST-GFP 4d MD, CamKII-Lypd6 4d MD: respectively, ** $P = 0.0477$, ** $P = 0.0183$, ** $P = 0.0073$. CamKII-Lypd6 4d MD does not differ from CamKII-Lypd6 no MD or CamKII-GFP-4d MD: respectively, $P = 0.9527$, and $P = 0.9969$; Tukey's multiple comparisons test). As a result, robust plasticity was measured only in the deprived mice that were overexpressing Lypd6 specifically in SST interneurons. Taken together, these results suggest that SST interneurons are

critical for reactivation of plasticity in adult V1 via Lypd6. Furthermore, the temporal and spatial restriction of viral injections implies that overexpression of Lypd6 directly in V1 after the closure of critical period plasticity is sufficient for the induction of robust plasticity.

α 2 nicotinic acetylcholine receptor subunit is required for reactivation of ocular dominance plasticity.

We next aimed to determine the nAChR subtype mediating the effect of Lypd6 in SST interneurons on V1 plasticity. In the hippocampus, SST-positive oriens-lacunosum (O-LM) interneurons that share similar characteristics to some SST expressing cortical Martinotti interneurons⁴⁸, express Lypd6 as well as α 2-containing nAChR (nAChR α 2), which is the most sparsely expressed nAChR subtype in the brain and features unique non-desensitizing characteristics^{39,42}. In the cortex, the punctate expression pattern of nAChR α 2 subunit in deep cortical layers⁴⁹ highly resembles that of Lypd6 expression⁴². Indeed, *in situ* hybridization of Lypd6 and nAChR α 2 revealed that 79% of cells labeled with nAChR α 2 also contain Lypd6, and that nAChR α 2 subunit is expressed on more than 53% of Lypd6 positive cells (Fig. 3a-c). Furthermore, while 23% of SST-positive cells overlapped with nAChR α 2 labeled cells, 95% of nAChR α 2 labeled cells overlapped with SST-positive cells (Fig. 3 d-f). No overlaps were observed between nAChR α 2 and VIP or vGlut1, the markers of vasoactive intestinal peptide interneuron and pyramidal cells (data not shown), consistent with a recent single cell RNA sequencing study in adult V1⁵⁰. Together this confirms strong overlapping expression of Lypd6 and nAChR α 2, preferentially in a subpopulation of SST interneurons.

Due to this high degree of co-localization and known modulation of non- α 7 nAChRs by Lypd6⁴³, we examined whether ablation of nAChR α 2 could eliminate the ocular dominance plasticity induced by adult SST-specific overexpression of Lypd6. To accomplish this, we created a bigenic SST-cre/Chrna2KO mouse line allowing for SST-specific Cre-recombinase expression on a background of nAChR α 2 knockout (Chrna2KO)⁵¹. We then injected AAV-Lypd6 into V1 of adult SST-cre/Chrna2KO

bigenic mice, allowed >3 weeks for viral incorporation, and assessed ocular dominance plasticity after 4d MD (Fig. 3d). Intriguingly, ablating nAChR α 2 (SST-Lypd6/ α 2KO 4d MD) eliminated the robust plasticity induced through SST-specific Lypd6 overexpression in adult V1. Unlike the adult SST-Lypd6 4d MD mice, adult SST-Lypd6/ α 2KO 4d MD mice, as well as deprived and non-deprived adult Chrna2KO mice (α 2KO 4d MD and α 2KO no MD) did not show significant OD shifts (Fig. 3e: SST-Lypd6/ α 2KO 4d MD vs. SST-Lypd6 4d MD: **** P <0.0001, vs. α 2KO 4d MD: P =0.62. α 2KO 4d MD vs. α 2KO no MD: P =0.24, χ^2 test), nor significant shifts of cumulative distributions of ODI (Fig. 3f: SST-Lypd6/ α 2KO 4d MD vs. SST-Lypd6 4d MD: **** P <0.0001, vs. α 2KO 4d MD: P =0.64. α 2KO 4d MD vs. α 2KO no MD: P =0.06, K-S test), nor decreases in CBI (Fig. 3g: ** P =0.0053, one-way ANOVA. SST-Lypd6/ α 2KO 4d MD is only significantly different with SST-Lypd6 4d MD: * P =0.0209, and is not different from α 2KO 4d MD: P =0.9990. α 2KO 4d MD vs. α 2KO no MD: P >0.9999; Tukey's multiple comparisons test). These findings strongly suggest the requirement of nAChR α 2 in the induction of plasticity by Lypd6 in SST interneurons.

To further investigate the physiological role of nAChR α 2 in regulating plasticity in adult V1, we turned to a condition known for modifying SST interneuron activity as well as reactivating V1 plasticity. Voluntary physical exercise through the use of a running wheel was recently shown to induce juvenile form of plasticity in adult mouse⁵². Interestingly, locomotion is also known to modulate SST interneuron activity²⁹⁻³³. We therefore examined the functional contribution of nAChR α 2 in this model of reactivation of V1 plasticity. When allowed voluntary exercise (+Running) on a running dish during the 4d MD (Fig. 3h), adult WT mice (WT 4d MD, +Running) displayed a significant shift in ocular dominance, consistent with a published study⁵². However, adult Chrna2KO mice that had undergone the same condition (α 2KO 4d MD, +Running) displayed neither OD shift (Fig. 3i: Chrna2KO 4d MD+Running vs. WT 4d MD+Running: **** P <0.0001, vs. Chrna2KO no MD+Running: P =0.35, χ^2 test), nor a shift in the cumulative distributions of ODI (Fig. 3j: Chrna2KO 4d MD+Running vs. WT 4d MD+Running: **** P <0.0001, vs. Chrna2KO no MD+Running: P =0.33, K-S test), nor a significant decrease in CBI (Fig.

3k: $**P=0.0030$, one-way ANOVA. The only significant differences observed were between WT 4d MD+Running and all other groups: Chrna2KO 4d MD+Running and Chrna2KO no MD+Running: respectively, $**P=0.0046$, $**P=0.0103$; Tukey's multiple comparisons test). Interestingly, SST-specific viral knockdown of Lypd6 in the adult V1 of voluntary-exercise-induced plasticity model displayed similar level of OD plasticity as adult WT 4d MD+Running mice (n=106 cells from 4 mice. $P=0.22$, χ^2 test; Sadahiro et al., unpublished data). We postulated that other members of the Lynx family played a compensational role in mediating voluntary-exercise-induced plasticity in the Lypd6 knockdown context. Alternatively, as the role of Lypd6 is that of a positive modulator of nAChRs, and given that knocking out Chrna2 could eliminate the voluntary-exercise-induced plasticity, simply knocking down Lypd6 may not be sufficient to block exercise induced-plasticity in the presence of nAChR $\alpha 2$. In addition, we performed qPCR on V1 extractions of adult WT 4d MD+Running mice (n=4) and control adult WT 4d MD (n=4) mice to examine if voluntary exercise changes the expression of Chrna2 or Lypd6, but did not find any significant expression level differences in either Chrna2 or Lypd6 (Chrna2: $P=0.7908$, Lypd6: $P=0.7111$ Student's *t*-test). We also compared Chrna2 expression between adult SST-Lypd6 no MD mice (n=2), and adult SST-GFP no MD mice (n=2), and did not detect any significant differences ($P=0.20$, Student's *t*-test). Perhaps increased cholinergic activity is sufficient to enhance nAChR $\alpha 2$ signaling and encourage voluntary-exercise-induced plasticity in the adult brain. Collectively, these results suggest that the voluntary-exercise-induced model of V1 plasticity requires nAChR $\alpha 2$, further signifying the critical role of nicotinic signaling through nAChR $\alpha 2$ in reactivating plasticity in adulthood.

Lypd6 expressed in SST interneurons increases their activity to drive ocular dominance plasticity.

Having ascertained that the effect of Lypd6 in reactivating V1 plasticity is regulated through SST interneurons, we investigated the plasticity mechanisms in these cells as well as downstream circuits. SST interneurons are known to provide inhibitory inputs onto PV interneurons in cortex^{28,53-57}, and

inhibit PV interneurons twice as potently as pyramidal neurons in mouse V1⁵⁸. As rapid reduction in PV interneuron firing, during the first day of MD, is a unique trigger of V1 plasticity during the critical period²², we examined whether adult overexpression of Lypd6 in SST interneurons can increase the activity of SST interneurons and in turn suppress PV activity during the first day of MD.

First, to directly evaluate how overexpression of Lypd6 in SST interneurons affects their activity, we used channelrhodopsin-2 (ChR2) as an optogenetic tag to identify any visually evoked single-unit responses as SST interneurons based on their time-locked optogenetic activation (Fig. 4a, b). We targeted expression of ChR2 specifically to SST interneurons by injecting AAV with Cre-dependent expression of ChR2 into adult SST-Cre mice along with either AAV-Lypd6 (SST-Lypd6) or AAV-GFP (SST-GFP) in adulthood (>P60) and, after >3 weeks of viral incorporation, subjected the mice to MD for a duration of 24 hours (1d MD) (Fig. 4c). Considering the physiological context of lypd6 expression in deep cortical layers, we restricted our analyses to only the SST interneurons recorded from the lower half of the 16-channel linear silicone probe in an effort to focus on the SST interneurons of lower layer IV, layers V, and VI. In adult SST-Lypd6 mice that underwent 1d MD (SST-Lypd6 1d MD), there was a significant increase in the visually evoked firing rate of SST interneurons compared to 1d MD adult SST-GFP mice (SST-GFP 1d MD) or non-deprived adult SST-Lypd6 (SST-Lypd6 no MD) mice when analyzed using a linear mixed model (LMM) that considers animal as a variable with random effect, and genetic manipulation (-GFP or -Lypd6) and experience (1d MD or no MD) as variables with fixed effects (Fig. 4d, e: SST-Lypd6 1d MD vs. SST-GFP 1d MD: $*P=0.0136$, vs. SST-Lypd6 no MD: $*P=0.0339$, LMM: for details See *Methods – Statistical analysis*). In comparing baseline firing rates, only a trending increase in firing rate was observed in SST-Lypd6 1d MD mice (4.47 spikes/sec) relative to SST-GFP 1d MD mice (2.87 spikes/sec) (SST-Lypd6 1d MD vs. SST-GFP 1d MD: $P=0.057$), and no significant difference was found when assessing experience-dependent effects (SST-Lypd6 1d MD vs. SST-Lypd6 no MD (4.77 spikes/sec): $P=0.97$, LMM). This result suggests an interactive effect of Lypd6 overexpression and sensory experience in rapidly increasing SST interneuron activity.

To then determine the causal role of rapid increases in SST interneuron activity itself in mediating plasticity, we examined if chemogenetic activation of SST interneurons strictly during the first day of deprivation can reactivate plasticity (Fig. 4f and Supplementary Fig. 3). Adult SST-cre mice were injected with an AAV with Cre-dependent expression of excitatory Gq protein-Designer Receptors Exclusively Activated by Designer Drugs (AAV8-hSyn-DIO-hM3D(Gq)-mCherry: AAV-GqDREADD)⁵⁹. In mice injected with Clozapine-N-Oxide (CNO) to activate SST interneurons during the first day of the 4d MD (CNO+), there was a significant OD shift compared with mice that received saline injections (CNO-) (Fig. 4g: *** $P=0.0007$, χ^2 test). The cumulative distributions of ODI show a significant shift in CNO+ mice compared to CNO- mice (Fig 4h: ** $P<0.0001$, K-S test). Comparisons of CBI scores show a significant decrease only when SST interneurons were activated by injection of CNO (Fig. 4i: * $P=0.0208$, Student's t -test). Together, these results imply a novel role for SST interneuron activity in reactivating a juvenile form of plasticity in adult V1.

Lypd6 expressed in SST interneurons suppresses PV interneuron activity to drive ocular dominance plasticity.

Finally, we aimed to elucidate the consequence of Lypd6-mediated elevation in SST activity, specifically upon PV interneuron activity. In adult SST-cre mice, we injected AAV-Lypd6 (SST-Lypd6) or AAV-GFP (SST-GFP) and, after >3 weeks of viral incorporation, subjected the mice to 1d MD (Fig. 5a). We putatively determined the cell-type identity of visually evoked PV interneurons using spike shape-based classification. Visually evoked cells were sorted into two categories: putative fast-spiking PV- (pFS) neurons, as defined by a characteristic narrow spike waveform, or regular-spiking neurons (RS) (Supplementary Fig. 2d, e).

In adult SST-Lypd6 mice that underwent 1d MD (SST-Lypd6 1d MD), use of standard binomial tests to compare cell-level means of pFS neuron firing rates confirmed a significant reduction compared to all control groups (Fig. 5c see legend). However, analysis using LMM showed a trending reduction

with no statistical significance (Fig. 5b, c: SST-Lypd6 1d MD vs. SST-GFP 1d MD: $P=0.211$, vs. SST-Lypd6 no MD: $P=0.2301$, vs. SST-GFP no MD: $P=0.1161$, LMM), likely reflecting a broad distribution of firing rates among pFS neurons. We therefore further subdivided the firing rates of the pFS neurons from each group into 6 categorical bins of 6 spikes/second each, ranging from 0 to 36 spikes/second, and found the distribution of the firing rates of pFS neurons of adult SST-Lypd6 1d MD mice to be significantly different from all controls, such that these mice had a higher amount of cells distributed towards the lowest firing rate category compared to all other groups (Fig. 5d: SST-Lypd6 1d MD vs. SST-GFP 1d MD: $***P=0.0009$, vs. SST-Lypd6 no MD: $*P=0.00454$, vs. SST-GFP no MD: $*P=0.0160$, χ^2 test). This suggests that 1d MD results in a decrease in visually evoked firing rate of pFS cells only when Lypd6 is overexpressed in adult SST interneurons. When strictly comparing the fraction of the lowest firing rate category to that of the second lowest firing rate category within each group, only the adult SST-Lypd6 1d MD mice had a significantly larger fraction of pFS cells in the lowest firing rate category compared to that of the second lowest firing rate category (Fig. 5e: $*P=0.0136$, Student's t -test). With respect to baseline firing rates, no significant differences were observed (SST-Lypd6 1d MD (2.06 spikes/sec) vs. SST-GFP 1d MD (2.55 spikes/sec): $P=0.86$, vs. SST-Lypd6 no MD (3.08 spikes/sec): $P=0.49$). Altogether these results may suggest an interactive effect of overexpression of Lypd6 and sensory experience in rapidly decreasing PV interneuron activity.

To determine the causal role of PV interneuron activity in robust plasticity regulated by Lypd6, we examined if chemogenetic restoration of PV interneuron activity during the first day of deprivation can prevent robust plasticity regulated by Lypd6 overexpression (Fig. 5d and Supplementary Fig. 4). Adult bigenic Lypd6Tg/PV-cre mice were injected with AAV-GqDREADD. In mice injected with CNO to activate PV interneurons during the first day of the 4d MD (CNO+), there was a significant blockage of ocular dominance plasticity compared with mice that received saline injections (CNO-) (Fig. 5g: $**P=0.0030$, χ^2 test). The cumulative distributions of ODI show that the shift is significantly eliminated in CNO+ mice compared to CNO- mice (Fig. 5h: $**P=0.0054$, K-S test). Comparisons of CBI scores show

a blockage of decrease only when PV interneurons were activated by injection of CNO (Fig. 5i: $*P=0.0128$, Student's *t*-test). While we cannot fully rule out the possibility that the suppression of V1 responses by the chemogenetic activation of PV interneurons partly contributed the blockage of plasticity, together these results implicate the role of Lypd6 in potentiating SST activity to engage an SST interneuron-based inhibition of PV interneurons, a novel inhibitory-inhibitory circuit, to induce a juvenile form of plasticity in the adult V1.

Discussion

Our study identified an endogenous nAChR modulator, Lypd6, and its action through nAChR α 2 as the first SST interneuron-specific molecular targets to reactivate plasticity in the adult cortex. As SST interneurons are known to be modulated by alteration of visual inputs²⁷, neuromodulation induced by locomotion²⁹⁻³³, or top-down regulation³⁴⁻³⁶, the Lypd6-nAChR α 2 system is ideally situated to gate these multiple modulatory inputs onto SST interneurons to regulate plasticity. Having demonstrated the Lypd6-nAChR α 2 system as a molecular target for restoring plasticity in the adult brain, it would be necessary in future studies to determine to what extent they are relevant in regulating plasticity in the juvenile cortex. Our study provides critical knowledge underlying the molecular and circuit means for the induction of plasticity in the adult visual cortex, which can unveil potential targets to help establish new therapeutic targets and strategies for the treatment of disorders with limited recovery potential due to diminished plasticity such as amblyopia.

Lypd6 as a novel plasticity regulator through nAChR α 2

Lypd6, like several members of the Lynx family⁴¹, is membrane tethered through a glycosylphosphatidylinositol (GPI)-anchor and is known to modulate nicotinic signaling⁴³. Our results from SST-specific Lypd6 overexpression on a background of ChR α 2 knockout suggest that the primary

mechanism for Lypd6-based initiation of plasticity is specifically mediated through nAChR α 2s. However, Lypd6 may also have additional activity unrelated to nicotinic signaling⁶⁰. While the subcellular localization of Lynx proteins has not been fully elucidated, there is evidence that they potentially localize to synaptic compartments to modulate nAChRs^{61 62}. Lypd6 may facilitate the activation of SST interneurons by impacting postsynaptic nicotinic modulation of excitatory synaptic input onto SST interneurons, such as in the case of hippocampus CA1 oriens-lacunosum where nAChR α 2 and their non-desensitizing features are critical for gating LTP through receptor-mediated calcium influx in SST interneurons³⁹. Alternatively, Lypd6 may modulate nicotinic signaling at presynaptic SST terminals to facilitate the release of GABA⁶³. Nevertheless, either potential mechanism may achieve the facilitation of activity of SST interneurons, a physiological condition that we confirmed, through chemogenetic activation of SST-interneurons, to be a trigger of robust plasticity (Fig. 4). While proper antibodies suited for immunohistochemical analyses are currently unavailable, application of recently developed technologies such as *in vivo* genome editing⁶⁴ that would allow labeling of endogenous Lypd6 or nAChR α 2 protein will reveal more mechanistic insight in future studies.

Deep layer cortical SST interneuron as a cellular target for nicotinic modulation of plasticity

Our study highlights Lypd6-nAChR α 2 expressing SST interneurons located in deep layers of V1 as a key cellular target for nicotinic neuromodulation to reactivate plasticity in adulthood. Previous studies have reported mixed results regarding the question of whether nicotinic signaling directly affects SST interneurons. While some studies reported clear nicotinic responses in neocortical SST interneurons^{65 66 28}, some have reported otherwise^{67 68}. The discrepancy may reflect the observation that expression of Lypd6 and nAChR α 2 is selective to a subpopulation of SST interneurons located in deep cortical layers (layers 5 and 6) but not to those in layer 2/3 (Fig.3)^{50 42}. It is possible that such a minor subpopulation of deep layer Lypd6-expressing SST interneurons was just not well represented in the previous negative reports. For example Gullledge et al.⁶⁶ reported that 30% of SST interneurons in layer

5 rat V1 responded to nicotine, which is consistent with the percentage of SST cells expressing Lypd6 and nAChR α 2. While the expression of Lypd6 and nAChR α 2 are limited to a subpopulation of deep layer cortical SST interneurons, the unique non-desensitizing nature of nAChR α 2 allows continual activation and calcium entry in the presence of Ach³⁹, making the nAChR α 2 highly suited for driving cortical plasticity by elevating nicotinic tone with Lypd6 or by triggering cholinergic inputs through locomotion. The SST-interneurons in deep cortical layers are also reported to project widely to almost all cortical layers and types of neurons⁶⁹, which can potentially contribute to widespread distribution of the drive for cortical plasticity exerted through nAChR α 2. Overall our study highlights the Lypd6-nAChR α 2 expressing SST interneuron as a cellular target of nicotinic neuromodulation to reactivate cortical plasticity in the adult V1. More mechanistic insight into the physiological action of ACh and Lypd6 on nAChR α 2 signaling in this selective population of SST interneurons can be expected in future studies by taking full advantage of the recently developed cre mouse lines targeting specific subpopulations of SST interneurons^{38 70} and combining with future development of a new ChAT-ChR2 transgenic mouse line that avoids confounding abnormally high cholinergic tone⁷¹, to allow proper optogenetic modulation of endogenous Ach release. The development of the selective nAChR α 2 antagonists for acute pharmacological modulation is also highly anticipated.

SST-PV disinhibition as a novel circuit for restoring juvenile form of plasticity in the adult

Our findings establish a novel circuit mechanism for triggering a juvenile form of plasticity in adulthood – through SST interneuron-mediated inhibition of PV interneurons. To our knowledge, this is the first evidence implicating the role of the SST-PV disinhibitory circuit in modulating cortical plasticity. We demonstrated that the overexpression of Lypd6 in SST interneurons leads to reduced PV interneuron activity, similar to what is typically observed only in juvenile mice after 1 day of visual deprivation²². Interestingly, a recent study showed that *silencing* of SST interneurons for the *entirety of 5 days of visual deprivation* can enhance some level of cortical plasticity in adulthood, but the nature of

plasticity measured was restricted as an adult form – an elevation of open ipsilateral eye response but no reduction of the deprived contralateral eye response, which is typically a hallmark of plasticity in juvenile mice ²⁶. Nevertheless, collectively these studies highlight the capabilities of SST interneurons in engaging both a homeostatic adult form of plasticity ²⁶ and a rapid form of juvenile like-plasticity ²², depending on the level of SST interneuron activity (reduced or activated) and the timing of activity change (during the initial phase of plasticity within 1 day or later homeostatic phase after 5 days) – a versatility reflected by the placement of the SST interneuron in the cortical circuit as an integrator of a variety of inputs. Consistently, recent studies demonstrated that SST interneurons in V1 can either be activated or suppressed by neuromodulatory inputs triggered by locomotion depending on the context of the visual environment ²⁹⁻³³. Specifically, locomotion enhances overall SST interneuron activity when the mouse is presented with large visual input ^{29,30} including a full-field gray screen ³¹. On the other hand, SST interneurons are largely non-responsive to small visual inputs ³⁰ or suppressed in darkness by the neuromodulatory activation of the VIP-SST circuit ^{29 32}. We propose a model whereby the Lypd6-nAChR α 2 system may function as a molecular switch board for SST interneurons to shift modes and activate the nAChR α 2-dependent SST-PV disinhibitory circuit, ^{38,72} to trigger a juvenile form of plasticity ²² while suppressing an adult form of plasticity, mainly through reduction of inhibitory action upon the distal dendrites of pyramidal neurons ^{26,73,74} that is normally engaged through an nAChR α 2-independent vasoactive intestinal peptide VIP-SST disinhibitory circuit ²⁶. In this model, both SST-PV and VIP-SST disinhibitory circuits can co-exist to play complementary roles in the modulation of plasticity, depending on the context and states of the adult brain. While SST interneurons are known to exhibit maturation towards the end of the critical period in V1⁷⁵, the differential contributions of SST-PV and VIP-SST circuits in regulating plasticity between critical period and adulthood remains unknown. It also remains to be determined how neuromodulation of SST interneurons changes from critical period to adulthood to regulate plasticity.

Lypd6-nAChR α 2 system as a potential therapeutic target for modulating plasticity in brain disorders

The potential for signaling through nAChR α 2 and its modulation by Lypd6 to induce plasticity in the adult cortex opens up the possibility of targeting these receptors for therapeutic interventions. The selective expression of Lypd6 and nAChR α 2 in SST interneurons make them attractive novel therapeutic targets with the potential of fewer off target effects ⁷⁶⁻⁷⁸ than interventions directed against more non-specific targets (more abundant nicotinic subunits) to treat conditions where recovery is limited due to diminished plasticity such as amblyopia, stroke, and traumatic brain injury. There are recent reports of positive allosteric modulators with much higher specificity for nAChR α 2 ⁷⁶⁻⁷⁸. Combinations of such pharmacological interventions with behavioral interventions like physical exercise ⁵² known to impact SST interneuron activity ^{29-32,79} (Fig. 3) may also become fruitful aims. Finally, our study highlights the disruption of cortical plasticity as a key pathophysiological consequence of either mutations of the *nAChR α 2* gene ^{80 81 82} and its non-coding regulatory elements ⁸³, or deficits in SST interneurons ^{84 85 86 87 88 89 90} increasingly reported in multiple neurodevelopmental, neurodegenerative, and psychiatric disorders including epilepsy, addiction, depression, and schizophrenia.

Methods

Animals.

All mice were housed in groups of 2–5 together with the sibling groups of the same sex in standard and uniform cage sizes (199 mm x 391 mm x 160 mm: width x depth x height, GM500, Tecniplast) under a 12hr light:dark cycle (lights on at 7:00AM: lights off at 7:00PM) in a facility with constant temperature (23°C) and ad libitum access to food and water. Wild-type C57Bl/6 mice were obtained from Jackson laboratory and Charles River. Both male and female were used. Lypd6Tg mice were originally generated by A.Z.⁴³, and transferred to H.M. and back-crossed to C57Bl/6. Somatostatin-ires-cre (SST-cre: Jackson laboratory #013044), Parvalbumin-ires-cre (PV-cre: Jackson laboratory #008069), and Chrnα2KO (MMRRC #30508) were purchased and bred in-house. Bigenic lines were created through targeting breeding of above strains. All animal protocols were approved by the Institutional Care and Use Committee (IACUC) at Icahn School of Medicine at Mount Sinai.

Monocular deprivation.

Adult mice (>P60) were anesthetized with isoflurane. Eyelid margins were trimmed using an iris scissor and one eye was sutured closed for one or four days. Following MD, mice were returned to their home cage prior to extracellular recording and subsequent euthanasia.

Generation and validation of AAV-Lypd6.

Lypd6 was amplified from a cDNA library derived from whole mouse V1, subcloned into a pcDNA3.1(-) vector using an isothermal DNA assembly method (Gibson Assembly; New England Biolabs) and transformed into *E. Coli*. Colonies with correct insert were identified through DNA sequencing (Genewiz), cultured and then isolated using a Hi-speed Midiprep kit (Qiagen). Expression was first examined by transfection of N2A cells *in vitro*. To create pAAV vector, an inverted bicistronic

2A sequence was inserted into pAAV-Ef1a-DIO-EGFP-WPRE-pA (Addgene#37084) upstream of EGFP by PCR linearization and overhang production on pAAV vector. The pcDNA3.1(-)-Lypd6 vector was used as a template for the Lypd6 insert which was subsequently inserted into the pAAV-DIO-EGFP-2A vector as described above to create a pAAV-DIO-EGFP-2A-Lypd6-WPRE-pA vector. After sequence verification, a large culture and Maxiprep isolation produced a purified vector that was sent to the UNC viral core for viral packaging using an AAV8 serotype. To confirm viral efficiency, AAV-Lypd6 was stereotactically injected (see below for injection methods) into V1 of SST-cre mice. After perfusion, sections were labeled with rabbit anti-somatostatin antibodies (1:1000; Peninsula Laboratories) and the SST-specific GFP expression was confirmed. V1 was micro-dissected from an additional cohort of mice to assay overexpression of Lypd6 through qPCR. RNA was isolated using an RNeasy lipid tissue mini kit (Qiagen) and cDNA was produced. The cDNA was subjected to qPCR analysis using a Taqman assay (Life Technologies) at the Icahn School of Medicine at Mount Sinai Quantitative PCR CORE facility.

Stereotaxic injection.

Mice were isoflurane anesthetized and head-fixed in a mouse stereotaxic apparatus (Narishige). A mid-line incision was made in the scalp and a micro-drill was used to drill a small hole in the skull over the right visual cortex. Three injections (0.5 μ l each) were made into the deep layers of V1 binocular zone (from lambda: AP: 0.0, ML: 3.1, DV: 0.6; AP: 0.0, ML: 2.85, DV: 0.6; AP: 0.3, ML: 3.0, DV: 0.6) using a 2.5 μ l syringe (Hamilton Company) with a 30-gauge needle and microsyringe pump controller (World Precision Instruments) set to inject at 200nl/minute. The syringe remained in place for one minute following injection to reduce backflow of virus. After injections, the skull hole was sealed using Kwik-Sil (World Precision Instruments), and the scalp was sutured. The mice were allowed to recover from anesthesia in an empty cage over a warming pad. Following recovery, mice were returned to their home cage where they remained for >3 weeks to allow for viral incorporation prior to any

additional procedures or testing. The following viral constructs were used in this study: AAV-Lypd6 (AAV8-EF1 α -DIO-EGFP-2A-Lypd6), AAV-GFP (AAV8-hSyn-DIO-EGFP) (University of North Carolina (UNC) vector core), AAV-CamKII-Cre (AAV8-CamKIIa-mCherry-Cre: UNC vector core), AAV-GqDREADD (AAV8-hSyn-DIO-hM3D(Gq)-mCherry: UNC vector core), and AAV-ChR2 (AAV2-Ef1a-DIO-hChR2(H134R)-mCherry-WPRE-pA: UNC vector core).

Chemogenetic activation of hM3d(Gq) Designer Receptors Exclusively Activated by Designer Drugs (DREADD).

Clozapine-N-Oxide (CNO; Sigma-Aldrich), a normally inert compound that specifically activates DREADD receptors, was prepared in 0.9% saline and injected i.p. into adult SST-Cre (Fig. 4f-i) or Lypd6Tg/PV-cre bigenic mice (Fig. 5d-g) at a concentration of 3 mg/kg. CNO or saline was injected immediately following MD and again 12 hours later for DREADD induced activation of SST or PV interneurons during the first day of MD following the previously validated protocol in mouse visual cortex²²(Supplementary Fig. 3, 4).

In vivo extracellular recording.

Recording was performed under nembutal/ chlorprothixene anesthesia as previously described⁴⁶. For animals that had been monocularly deprived, under anesthesia the deprived contralateral eye was reopened just prior to the start of recordings. Visually evoked single-unit responses were recorded in response to a high contrast single bar, generated by Visage System (Cambridge Research Systems), that laterally traveled across the monitor in a 4 second interval followed by a 5 second interstimulus interval per trial. The stimulus was separately presented, by the use of an eye patch, first to the deprived eye and then to the open eye for 12 trials each. For each animal, 3 to 10 single units were recorded in each of the 4 to 6 vertical penetrations spaced evenly (250

μm intervals) across mediolateral extent of V1 to map the monocular and binocular zones to avoid sampling bias. A linear 16-channel electrode was used to record vertical penetrations, which allowed to record with similar weight from upper (channels 1~8) and lower (channels 1~9) cortical layers. By analyzing 7 of the experimental groups that were used in our data, we found that the fraction of neurons recorded from Upper Layers=0.5235 ± 0.02350 and Lower Layers=0.4765 ± 0.02350 (n=35 animals: $P=0.3247$, Student's t-test for paired samples). The signal was amplified and thresholded (OmniPlex, Plexon). To ensure single-unit isolation, the waveforms of recorded units were further examined offline (Offline Sorter, Plexon). To analyze the electrophysiology data, normalized OD index of single neuron was computed by custom made MATLAB program by peristimulus time histogram analysis of peak to baseline spiking activity in response to each eye: $\{[\text{Peak(ipsi)} - \text{baseline (ipsi)}] - [\text{Peak (contra)} - \text{baseline(contra)}]\} / \{[\text{Peak (ipsi)} - \text{baseline(ipsi)}] + [\text{Peak(contra)} - \text{baseline(contra)}]\}$. OD scores were converted from OD index using a 7-point classification scheme as follows: -1 to -0.5 = 1, -0.5 to -0.3 = 2, -0.3 to -0.1 = 3, -0.1 to 0.1 = 4, 0.1 to 0.3 = 5, 0.3 to 0.5 = 6, 0.5 to 1 = 7. For each binocular zone, contralateral bias index (CBI) is calculated according to the formula: $[(n1-n7)+2/3(n2-n6)+1/3(n3-n5)+N] / 2N$, where N=total number of cells and n_x =# of cells corresponding to OD score of x.

For optical tagging experiments, SST interneurons were optogenetically tagged by injecting a Cre-dependent virus expressing channelrhodopsin-2 (AAV2-Ef1a-DIO-hChR2(H134R)-mCherry-WPRE-pA: UNC Vector Core) into the V1 binocular zone of SST-cre mice. The expression of channelrhodopsin in a cell-type of interest allowed the use of optogenetic stimulation with a blue light as a search stimulus to simultaneously sort stimulus-locked responses from cell-types of interest, and then record their visually evoked responses, by using an optic fiber-coupled 16-channel linear silicone probe (Neuronexus). This allowed accurate and high-throughput recordings of specific cell-types, even against broad baseline noise and activities of other neuronal populations. Optogenetically tagged SST interneurons of the V1 binocular zone were identified using a 473 nm (blue) laser search stimulus emitted and delivered through the optic fiber coupled to the silicone probe and oriented immediately

above the V1 cortical surface. After sorting for optogenetically responsive units (SST interneurons expressing ChR2), the optogenetic stimulus was switched off. Then a high-contrast single bar visual stimulus was presented to each eye to record the visual evoked responses (spike firing rate) of the sorted units. To analyze the SST interneuron visually evoked firing rates, normalized firing rate was computed by first using a custom made MATLAB program to generate a peristimulus time histogram-based analysis of peak and baseline spiking activity in response to visual stimulus. The peak activity was then subtracted by baseline spiking activity in order to obtain the normalized visually evoked firing rate. The normalized firing rates of SST interneurons from each experimental condition were then pooled and averaged, and finally compared between groups.

To isolate visually evoked responses from putative fast-spiking (pFS) neurons, visual stimulus responsive cells were distinguished as pFS neurons or regular-spiking (RS) neurons by means of spike width- (trough-to-peak time) based classification. The spike-width criterion for separating into pFS and RS neurons was established by measuring the spike width of optogenetically tagged PV interneurons. PV interneurons were optogenetically tagged by injecting a Cre-dependent virus expressing channelrhodopsin-2 (AAV2-Ef1a-DIO-hChR2(H134R)-mCherry-WPRE-pA, UNC Vector Core) into V1 binocular zone of PV-cre mice. During recording, PV interneurons were first identified and sorted, using a 473 nm laser search stimulus delivered through the optical fiber coupled to the 16-channel silicone probe and oriented immediately above the V1 cortical surface, depending on their responsiveness to blue light stimulation within 3 msec post blue light emission. The search stimulus was then exchanged to a visual stimulus. Visually evoked spike widths of the PV interneurons identified by optical tagging were then pooled to establish the official criterion for pFS neurons as having visually evoked spike width time (trough-to-peak time) of less than 412 μ sec (Supplementary Fig. 2). Averaged spike waveform data for each unit was analyzed using a custom made MATLAB program to obtain a spike width time for each unit.

All AAV injected mice were transcardially perfused following recording and the extent of GFP or mCherry signal was utilized to assess the viral transduction. Only mice that exhibited GFP or mCherry signal in the recorded V1 area were included for the analysis of ocular dominance plasticity.

In situ hybridization.

The production of probes and methodology for *in situ* hybridization has been previously described⁴². Briefly, RNA probes including a fluorescein or digoxinogen (DIG) tag were generated and utilized to label *Lypd6*, *SST*, *VIP*, *vGlut1*, *GFP*, and *nAChRa2* mRNA in 7 μ m sections of V1 from fresh frozen brains of animals at P28 (CP) and >P60 (adult). To fluorescently label mRNA, anti-fluorescein/DIG-POD (1:2000; Roche) and anti-fluorescein/DIG-Alkaline phosphatase (AP) (1:1000; Roche) antibodies were used. POD-conjugated antibody labeling of mRNA was proceeded with with TSA Plus DNP signal amplification (Perkin Elmer) and a subsequently labeling with anti-DNP-KLH-488 antibodies (1:1000; Life Technologies). AP-conjugated-antibody-labeled mRNA was stained using HNPP/Fast Red (Roche). Imaging was performed using an LSM780 confocal microscope (Zeiss). ImageJ was used to quantify the density of labeled pixels from each image or to examine co-localization using a color based thresholding method. For the quantification of *Lypd6* mRNA expression across age in V1, pixel density (>2 standard deviations above mean intensity of full image field) was determined from low magnification images of V1 binocular zone using ImageJ software. For the quantification of co-localization of *Lypd6* or *SST* or *VIP* with *nAChRa2*, the number of cells positive for *Lypd6*/*SST*/*VIP* or *nAChRa2* in each image was determined using ImageJ by automated counting using a threshold of >2 standard deviations above background and limiting to particles of >40 μ m cell diameter. To calculate the co-localization percentage, first color based thresholding was utilized in ImageJ to isolate and quantify the co-localized cells, then percentage was calculated by dividing the number of co-localized cells by the number of *Lypd6*/*SST*/*VIP* or *nAChRa2* positive cells in each image. For the quantification of co-localization of *GFP* and *vGlut1* mRNA, thresholding was first utilized to

isolate and calculate number of particles representing *GFP* labeled cells (>40 μm cell diameter). Then the corresponding *vGlut1* labeled image was redirected to the mask retained from the analysis of *GFP* labeled image to calculate total number and then percentage of *GFP* labeled cells with co-localized *vGlut1* labeling. For the quantification of *Lypd6* mRNA expression in V1 binocular zone of mice injected with a cocktail of AAV-DIO-Lypd6 and AAV-CamKII-Cre, low magnification images of binocular V1 from the injected or the corresponding naïve hemisphere were analyzed for particles after thresholding. Absolute intensity for each particle was then measured as the product of mean intensity and area of particle. All absolute intensity values were summed to obtain total binocular V1 intensity, which was subsequently normalized by dividing by the μm^2 area of the V1 binocular zone. The V1 binocular zone of each image was assessed using Paxinos and Franklin's The Mouse Brain in Stereotaxic Coordinates (1997) as reference.

Quantitative PCR (qPCR)

Adult mice were deeply anesthetized with isoflurane, checked for response with paw pinch, and decapitated. The brain was extracted, and under RNase- free conditions, briefly washed in ice cold 0.1 M phosphate buffer, and then an estimated area of cortical tissue representing V1 – a 2mm-by-2mm area of the cortex most posterior and 2mm lateral from the median, was cut out, white matter removed, immediately frozen on dry ice, and stored under -80°C . Total RNA was extracted from V1 using the RNeasy Mini Kit (Qiagen) and stored at -80°C . concentrations of total V1 RNA yielded ranged from 0.22 to 0.3 $\mu\text{g}/\mu\text{l}$. Total V1 RNA was converted to cDNA using a High- Capacity cDNA Reverse Transcription Kit (Life Technologies). qPCR was performed at the Mount Sinai Quantitative PCR core facility using 7900HT Real-Time PCR instrument (ABI/Life Technologies), TaqMan probes (catalog numbers: *Lypd6* Mm00622636_01, *Chrna2* Mm00460630_m1, ABI/Life Technologies) and TaqMan Universal Master Mix II, no UNG (ABI/Life Technologies). Quantification of the fold change was calculated via the $-\Delta\Delta\text{CT}$

method (equivalent to a log2 fold change), using Δ CT values derived by normalization of CT values to mouse beta actin as reference housekeeping gene.

Immunohistochemistry

Anesthetized mice were transcardially perfused with cold 4% paraformaldehyde (PFA) dissolved in 0.1M phosphate buffer. The brains were post-fixed in 4% PFA at 4 °C, and cryoprotected in 30% sucrose solution. The frozen brains were sectioned into 30- μ m-thick coronal sections using a cryostat (CM3050, Leica). Free-floating sections were washed in tris-buffered saline (TBS), pH 7.5, and then blocked in 1% bovine serum albumin in TBST (0.25% Triton X-100 in TBS) for 1 h. The sections were incubated with mouse anti-parvalbumin (1:500; Swant), rabbit anti-somatostatin (1:1000; Peninsula Laboratories), or rabbit anti-c-Fos (1:500; Calbiochem) antibodies overnight at room temperature. After primary antibody incubation the slices were washed in TBST, followed by secondary antibody incubation with Alexa fluor dyes (Thermo Fisher Scientific). Imaging was performed using a Zeiss LSM780 confocal microscope at 20 or 40X magnification. The investigator performing the analysis was blind to the animal genotype.

Statistical analysis.

The following statistical approaches were utilized for experiments assessing ocular dominance plasticity. χ^2 test was used to compare at cell level distributions of ocular dominance scores between two groups and assess for ocular dominance shift. For readability, the histogram figures for distribution of ocular dominance scores (OD Scores) represent percentage of cells rather than actual cell number. However the χ^2 statistics are results of the tests conducted on actual cell number. Cumulative distributions of ocular dominance index (ODI) were compared at cell level by using the Kolmogorov-Smirnov (K-S) test. One-way analysis of variance (ANOVA) was used to compare contralateral bias

index (CBI) at animal levels and Tukey's multiple comparisons test was used for post hoc analyses. As justification of the use of a parametric test, normality of the CBI data was tested by using the D'Agostino-Pearson Test and Shapiro-Wilk Test on any groups where n =mice exceeding the criteria for the tests ($n > 8$, and $n > 7$ respectively). Normality was confirmed in all groups where the test was applicable: WT MD, WT no MD, Lypd6 Tg 4d MD, and SST-Lypd6 4d MD. In addition, we applied the Shapiro-Wilk Test to the CBI data of a key experimental group from our previous study (Smith et al., 2016) that utilized the same experimental design and statistical analyses for testing ocular dominance plasticity, and also confirmed normality. Initial comparison of pFS cell (PV interneuron) and SST interneuron firing rates were conducted using one-way ANOVA with Bonferroni corrected multiple comparison tests for post hoc analyses. To officially determine the significance of difference in SST and PV interneuron firing rates, a linear mixed modeling approach was used, from packages LmerTest (v. 2.0.32), lme4 (v. 1.1.12), and lsmeans (v. 2.25) in the R programming language (v. 3.2.2). This model considered "animal" as a variable with random effect, and "genetic manipulation" (-GFP or -Lypd6) and "experience" (1d MD or no MD) as variables with fixed effects. Frequency distributions of firing rates in putative PV interneurons were compared between groups using χ^2 test. While figure is represented by fractions of whole, χ^2 statistics are results of the tests conducted on actual cell number. For all other experiments including quantification of expression, mean differences between two groups were determined using Student's *t*-test. A minimum *P* value of 0.05 was accepted as statistically significant. Other than LMM, all other statistical analyses were performed using Prism 6.0h (GrapPad Software). All CBI, quantified expression, quantified co-localization, and visually evoked firing rate data are presented in figures as mean \pm SEM.

Acknowledgments: This work was supported by National Eye Institute R01EY024918, R01EY026053, R21EY026702 to H.M., National Institute on Drug Abuse T32 DA007135 to M.P.D., National Institute of Mental Health T32MH096678 to M.S., Knights Templar Eye Foundation to H.M., March of

657 Dimes to H.M., Whitehall Foundation to H.M., and Brain and Behavior Research Foundation to H.M. AZ
 658 is a member of the Excellence Cluster Immunosensation. We thank Dr. Ming-Hu Han (Icahn School of
 659 Medicine at Mount Sinai) for providing technical expertise on optogenetics; Dr. Yasmin Hurd and Dr.
 660 Michael Michaelides (Icahn School of Medicine at Mount Sinai) for their expertise on chemogenomics.

661

662 **Author Contributions:** M.S., M.P.D., and H.M. designed research; M.S., M.P.D, P.N.B., **P.Y.**, and H.M.
 663 performed research; A.Z. contributed unpublished reagents and provided expertise; M.S., M.P.D,
 664 P.N.B., P.Y., M.R.S., and H.M. analyzed data; M.S., M.P.D, and H.M. wrote the paper.

665

References:

- 1 Hensch, T. K. Critical period regulation. *Annual review of neuroscience* **27**, 549-579, doi:10.1146/annurev.neuro.27.070203.144327 (2004).
- 2 Knudsen, E. I. Sensitive periods in the development of the brain and behavior. *Journal of cognitive neuroscience* **16**, 1412-1425, doi:10.1162/0898929042304796 (2004).
- 3 Wiesel, T. N. Postnatal development of the visual cortex and the influence of environment. *Nature* **299**, 583-591 (1982).
- 4 Espinosa, J. S. & Stryker, M. P. Development and plasticity of the primary visual cortex. *Neuron* **75**, 230-249, doi:10.1016/j.neuron.2012.06.009 (2012).
- 5 Morishita, H. & Hensch, T. K. Critical period revisited: impact on vision. *Current opinion in neurobiology* **18**, 101-107, doi:10.1016/j.conb.2008.05.009 (2008).
- 6 Hubener, M. & Bonhoeffer, T. Neuronal plasticity: beyond the critical period. *Cell* **159**, 727-737, doi:10.1016/j.cell.2014.10.035 (2014).
- 7 Levelt, C. N. & Hubener, M. Critical-period plasticity in the visual cortex. *Annual review of neuroscience* **35**, 309-330, doi:10.1146/annurev-neuro-061010-113813 (2012).
- 8 Deidda, G. *et al.* Early depolarizing GABA controls critical-period plasticity in the rat visual cortex. *Nature neuroscience* **18**, 87-96, doi:10.1038/nn.3890 (2015).
- 9 Huang, Z. J. *et al.* BDNF regulates the maturation of inhibition and the critical period of plasticity in mouse visual cortex. *Cell* **98**, 739-755 (1999).
- 10 Hanover, J. L., Huang, Z. J., Tonegawa, S. & Stryker, M. P. Brain-derived neurotrophic factor overexpression induces precocious critical period in mouse visual cortex. *The Journal of neuroscience : the official journal of the Society for Neuroscience* **19**, RC40 (1999).
- 11 Fagiolini, M. & Hensch, T. K. Inhibitory threshold for critical-period activation in primary visual cortex. *Nature* **404**, 183-186, doi:10.1038/35004582 (2000).
- 12 Chattopadhyaya, B. *et al.* GAD67-mediated GABA synthesis and signaling regulate inhibitory synaptic innervation in the visual cortex. *Neuron* **54**, 889-903, doi:10.1016/j.neuron.2007.05.015 (2007).
- 13 Iwai, Y., Fagiolini, M., Obata, K. & Hensch, T. K. Rapid critical period induction by tonic inhibition in visual cortex. *The Journal of neuroscience : the official journal of the Society for Neuroscience* **23**, 6695-6702 (2003).
- 14 Hensch, T. K. *et al.* Local GABA circuit control of experience-dependent plasticity in developing visual cortex. *Science* **282**, 1504-1508 (1998).
- 15 Sugiyama, S. *et al.* Experience-dependent transfer of Otx2 homeoprotein into the visual cortex activates postnatal plasticity. *Cell* **134**, 508-520, doi:10.1016/j.cell.2008.05.054 (2008).

- 700 16 Hensch, T. K. Critical period plasticity in local cortical circuits. *Nature reviews. Neuroscience* **6**,
701 877-888, doi:10.1038/nrn1787 (2005).
- 702 17 Harauzov, A. *et al.* Reducing intracortical inhibition in the adult visual cortex promotes ocular
703 dominance plasticity. *The Journal of neuroscience : the official journal of the Society for*
704 *Neuroscience* **30**, 361-371, doi:10.1523/JNEUROSCI.2233-09.2010 (2010).
- 705 18 Southwell, D. G., Froemke, R. C., Alvarez-Buylla, A., Stryker, M. P. & Gandhi, S. P. Cortical
706 plasticity induced by inhibitory neuron transplantation. *Science* **327**, 1145-1148,
707 doi:10.1126/science.1183962 (2010).
- 708 19 Tang, Y., Stryker, M. P., Alvarez-Buylla, A. & Espinosa, J. S. Cortical plasticity induced by
709 transplantation of embryonic somatostatin or parvalbumin interneurons. *Proceedings of the*
710 *National Academy of Sciences of the United States of America* **111**, 18339-18344,
711 doi:10.1073/pnas.1421844112 (2014).
- 712 20 Davis, M. F. *et al.* Inhibitory Neuron Transplantation into Adult Visual Cortex Creates a New
713 Critical Period that Rescues Impaired Vision. *Neuron* **86**, 1055-1066,
714 doi:10.1016/j.neuron.2015.03.062 (2015).
- 715 21 Yazaki-Sugiyama, Y., Kang, S., Cateau, H., Fukai, T. & Hensch, T. K. Bidirectional plasticity in
716 fast-spiking GABA circuits by visual experience. *Nature* **462**, 218-221, doi:10.1038/nature08485
717 (2009).
- 718 22 Kuhlman, S. J. *et al.* A disinhibitory microcircuit initiates critical-period plasticity in the visual
719 cortex. *Nature* **501**, 543-546, doi:10.1038/nature12485 (2013).
- 720 23 Pizzorusso, T. *et al.* Reactivation of ocular dominance plasticity in the adult visual cortex.
721 *Science* **298**, 1248-1251, doi:10.1126/science.1072699 (2002).
- 722 24 Beurdeley, M. *et al.* Otx2 binding to perineuronal nets persistently regulates plasticity in the
723 mature visual cortex. *The Journal of neuroscience : the official journal of the Society for*
724 *Neuroscience* **32**, 9429-9437, doi:10.1523/JNEUROSCI.0394-12.2012 (2012).
- 725 25 Rudy, B., Fishell, G., Lee, S. & Hjerling-Leffler, J. Three groups of interneurons account for
726 nearly 100% of neocortical GABAergic neurons. *Developmental neurobiology* **71**, 45-61,
727 doi:10.1002/dneu.20853 (2011).
- 728 26 Fu, Y., Kaneko, M., Tang, Y., Alvarez-Buylla, A. & Stryker, M. P. A cortical disinhibitory circuit
729 for enhancing adult plasticity. *eLife* **4**, e05558, doi:10.7554/eLife.05558 (2015).
- 730 27 Tan, Z., Hu, H., Huang, Z. J. & Agmon, A. Robust but delayed thalamocortical activation of
731 dendritic-targeting inhibitory interneurons. *Proceedings of the National Academy of Sciences of*
732 *the United States of America* **105**, 2187-2192, doi:10.1073/pnas.0710628105 (2008).
- 733 28 Chen, N., Sugihara, H. & Sur, M. An acetylcholine-activated microcircuit drives temporal
734 dynamics of cortical activity. *Nature neuroscience* **18**, 892-902, doi:10.1038/nn.4002 (2015).
- 735 29 Pakan, J. M. *et al.* Behavioral-state modulation of inhibition is context-dependent and cell type
736 specific in mouse visual cortex. *eLife* **5**, doi:10.7554/eLife.14985 (2016).

- 737 30 Dipoppa, M. *et al.* Vision and locomotion shape the interactions between neuron types in mouse
738 visual cortex. *bioRxiv*, doi:10.1101/058396 (2016).
- 739 31 Polack, P. O., Friedman, J. & Golshani, P. Cellular mechanisms of brain state-dependent gain
740 modulation in visual cortex. *Nature neuroscience* **16**, 1331-1339, doi:10.1038/nn.3464 (2013).
- 741 32 Fu, Y. *et al.* A cortical circuit for gain control by behavioral state. *Cell* **156**, 1139-1152,
742 doi:10.1016/j.cell.2014.01.050 (2014).
- 743 33 Reimer, J. *et al.* Pupil fluctuations track fast switching of cortical states during quiet
744 wakefulness. *Neuron* **84**, 355-362, doi:10.1016/j.neuron.2014.09.033 (2014).
- 745 34 Zhang, S. *et al.* Selective attention. Long-range and local circuits for top-down modulation of
746 visual cortex processing. *Science* **345**, 660-665, doi:10.1126/science.1254126 (2014).
- 747 35 Lee, S., Kruglikov, I., Huang, Z. J., Fishell, G. & Rudy, B. A disinhibitory circuit mediates motor
748 integration in the somatosensory cortex. *Nature neuroscience* **16**, 1662-1670,
749 doi:10.1038/nn.3544 (2013).
- 750 36 Makino, H. & Komiyama, T. Learning enhances the relative impact of top-down processing in
751 the visual cortex. *Nature neuroscience* **18**, 1116-1122, doi:10.1038/nn.4061 (2015).
- 752 37 Zhao-Shea, R., Liu, L., Pang, X., Gardner, P. D. & Tapper, A. R. Activation of GABAergic
753 neurons in the interpeduncular nucleus triggers physical nicotine withdrawal symptoms. *Current*
754 *biology : CB* **23**, 2327-2335, doi:10.1016/j.cub.2013.09.041 (2013).
- 755 38 Leao, R. N. *et al.* OLM interneurons differentially modulate CA3 and entorhinal inputs to
756 hippocampal CA1 neurons. *Nature neuroscience* **15**, 1524-1530, doi:10.1038/nn.3235 (2012).
- 757 39 Jia, Y., Yamazaki, Y., Nakauchi, S., Ito, K. & Sumikawa, K. Nicotine facilitates long-term
758 potentiation induction in oriens-lacunosum moleculare cells via Ca²⁺ entry through non- α 7
759 nicotinic acetylcholine receptors. *The European journal of neuroscience* **31**, 463-476,
760 doi:10.1111/j.1460-9568.2009.07058.x (2010).
- 761 40 Morishita, H., Miwa, J. M., Heintz, N. & Hensch, T. K. Lynx1, a cholinergic brake, limits plasticity
762 in adult visual cortex. *Science* **330**, 1238-1240, doi:10.1126/science.1195320 (2010).
- 763 41 Miwa, J. M., Lester, H. A. & Walz, A. Optimizing cholinergic tone through lynx modulators of
764 nicotinic receptors: implications for plasticity and nicotine addiction. *Physiology (Bethesda)* **27**,
765 187-199, doi:10.1152/physiol.00002.2012 (2012).
- 766 42 Demars, M. P. & Morishita, H. Cortical parvalbumin and somatostatin GABA neurons express
767 distinct endogenous modulators of nicotinic acetylcholine receptors. *Molecular brain* **7**, 75,
768 doi:10.1186/s13041-014-0075-9 (2014).
- 769 43 Darvas, M. *et al.* Modulation of the Ca²⁺ conductance of nicotinic acetylcholine receptors by
770 Lypd6. *European neuropsychopharmacology : the journal of the European College of*
771 *Neuropsychopharmacology* **19**, 670-681, doi:10.1016/j.euroneuro.2009.03.007 (2009).

- 772 44 Miwa, J. M. *et al.* The prototoxin lynx1 acts on nicotinic acetylcholine receptors to balance
773 neuronal activity and survival in vivo. *Neuron* **51**, 587-600, doi:10.1016/j.neuron.2006.07.025
774 (2006).
- 775 45 Sadahiro, M., Sajo, M. & Morishita, H. Nicotinic regulation of experience-dependent plasticity in
776 visual cortex. *Journal of physiology, Paris* **110**, 29-36, doi:10.1016/j.jphysparis.2016.11.003
777 (2016).
- 778 46 Bukhari, N. *et al.* Unmasking Proteolytic Activity for Adult Visual Cortex Plasticity by the
779 Removal of Lynx1. *The Journal of neuroscience : the official journal of the Society for*
780 *Neuroscience* **35**, 12693-12702, doi:10.1523/JNEUROSCI.4315-14.2015 (2015).
- 781 47 Koike, H. *et al.* Chemogenetic Inactivation of Dorsal Anterior Cingulate Cortex Neurons Disrupts
782 Attentional Behavior in Mouse. *Neuropsychopharmacology : official publication of the American*
783 *College of Neuropsychopharmacology* **41**, 1014-1023, doi:10.1038/npp.2015.229 (2016).
- 784 48 Heys, J. G., Schultheiss, N. W., Shay, C. F., Tsuno, Y. & Hasselmo, M. E. Effects of
785 acetylcholine on neuronal properties in entorhinal cortex. *Frontiers in behavioral neuroscience*
786 **6**, 32, doi:10.3389/fnbeh.2012.00032 (2012).
- 787 49 Ishii, K., Wong, J. K. & Sumikawa, K. Comparison of alpha2 nicotinic acetylcholine receptor
788 subunit mRNA expression in the central nervous system of rats and mice. *The Journal of*
789 *comparative neurology* **493**, 241-260, doi:10.1002/cne.20762 (2005).
- 790 50 Tasic, B. *et al.* Adult mouse cortical cell taxonomy revealed by single cell transcriptomics.
791 *Nature neuroscience* **19**, 335-346, doi:10.1038/nn.4216 (2016).
- 792 51 Lotfipour, S. *et al.* Targeted deletion of the mouse alpha2 nicotinic acetylcholine receptor
793 subunit gene (Chrna2) potentiates nicotine-modulated behaviors. *The Journal of neuroscience :*
794 *the official journal of the Society for Neuroscience* **33**, 7728-7741,
795 doi:10.1523/JNEUROSCI.4731-12.2013 (2013).
- 796 52 Kalogeraki, E., Greifzu, F., Haack, F. & Lowel, S. Voluntary physical exercise promotes ocular
797 dominance plasticity in adult mouse primary visual cortex. *The Journal of neuroscience : the*
798 *official journal of the Society for Neuroscience* **34**, 15476-15481,
799 doi:10.1523/JNEUROSCI.2678-14.2014 (2014).
- 800 53 Hioki, H. *et al.* Cell type-specific inhibitory inputs to dendritic and somatic compartments of
801 parvalbumin-expressing neocortical interneuron. *The Journal of neuroscience : the official*
802 *journal of the Society for Neuroscience* **33**, 544-555, doi:10.1523/JNEUROSCI.2255-12.2013
803 (2013).
- 804 54 Pfeffer, C. K., Xue, M., He, M., Huang, Z. J. & Scanziani, M. Inhibition of inhibition in visual
805 cortex: the logic of connections between molecularly distinct interneurons. *Nature neuroscience*
806 **16**, 1068-1076, doi:10.1038/nn.3446 (2013).
- 807 55 Xu, H., Jeong, H. Y., Tremblay, R. & Rudy, B. Neocortical somatostatin-expressing GABAergic
808 interneurons disinhibit the thalamorecipient layer 4. *Neuron* **77**, 155-167,
809 doi:10.1016/j.neuron.2012.11.004 (2013).

- 810 56 Sturgill, J. F. & Isaacson, J. S. Somatostatin cells regulate sensory response fidelity via
811 subtractive inhibition in olfactory cortex. *Nature neuroscience* **18**, 531-535, doi:10.1038/nn.3971
812 (2015).
- 813 57 Hu, H., Ma, Y. & Agmon, A. Submillisecond firing synchrony between different subtypes of
814 cortical interneurons connected chemically but not electrically. *The Journal of neuroscience : the*
815 *official journal of the Society for Neuroscience* **31**, 3351-3361, doi:10.1523/JNEUROSCI.4881-
816 10.2011 (2011).
- 817 58 Cottam, J. C., Smith, S. L. & Hausser, M. Target-specific effects of somatostatin-expressing
818 interneurons on neocortical visual processing. *The Journal of neuroscience : the official journal*
819 *of the Society for Neuroscience* **33**, 19567-19578, doi:10.1523/JNEUROSCI.2624-13.2013
820 (2013).
- 821 59 Urban, D. J. & Roth, B. L. DREADDs (designer receptors exclusively activated by designer
822 drugs): chemogenetic tools with therapeutic utility. *Annual review of pharmacology and*
823 *toxicology* **55**, 399-417, doi:10.1146/annurev-pharmtox-010814-124803 (2015).
- 824 60 Ozhan, G. *et al.* Lypd6 enhances Wnt/beta-catenin signaling by promoting Lrp6 phosphorylation
825 in raft plasma membrane domains. *Developmental cell* **26**, 331-345,
826 doi:10.1016/j.devcel.2013.07.020 (2013).
- 827 61 Thomsen, M. S. *et al.* Expression of the Ly-6 family proteins Lynx1 and Ly6H in the rat brain is
828 compartmentalized, cell-type specific, and developmentally regulated. *Brain structure & function*
829 **219**, 1923-1934, doi:10.1007/s00429-013-0611-x (2014).
- 830 62 Arvaniti, M. *et al.* Functional interaction between Lypd6 and nicotinic acetylcholine receptors.
831 *Journal of neurochemistry* **138**, 806-820, doi:10.1111/jnc.13718 (2016).
- 832 63 Marchi, M. & Grilli, M. Presynaptic nicotinic receptors modulating neurotransmitter release in the
833 central nervous system: functional interactions with other coexisting receptors. *Progress in*
834 *neurobiology* **92**, 105-111, doi:10.1016/j.pneurobio.2010.06.004 (2010).
- 835 64 Mikuni, T., Nishiyama, J., Sun, Y., Kamasawa, N. & Yasuda, R. High-Throughput, High-
836 Resolution Mapping of Protein Localization in Mammalian Brain by In Vivo Genome Editing. *Cell*
837 **165**, 1803-1817, doi:10.1016/j.cell.2016.04.044 (2016).
- 838 65 Poorthuis, R. B., Bloem, B., Verhoog, M. B. & Mansvelder, H. D. Layer-specific interference with
839 cholinergic signaling in the prefrontal cortex by smoking concentrations of nicotine. *The Journal*
840 *of neuroscience : the official journal of the Society for Neuroscience* **33**, 4843-4853,
841 doi:10.1523/JNEUROSCI.5012-12.2013 (2013).
- 842 66 Gullledge, A. T., Park, S. B., Kawaguchi, Y. & Stuart, G. J. Heterogeneity of phasic cholinergic
843 signaling in neocortical neurons. *Journal of neurophysiology* **97**, 2215-2229,
844 doi:10.1152/jn.00493.2006 (2007).
- 845 67 Porter, J. T. *et al.* Selective excitation of subtypes of neocortical interneurons by nicotinic
846 receptors. *The Journal of neuroscience : the official journal of the Society for Neuroscience* **19**,
847 5228-5235 (1999).

- 848 68 Alitto, H. J. & Dan, Y. Cell-type-specific modulation of neocortical activity by basal forebrain
849 input. *Frontiers in systems neuroscience* **6**, 79, doi:10.3389/fnsys.2012.00079 (2012).
- 850 69 Jiang, X. *et al.* Principles of connectivity among morphologically defined cell types in adult
851 neocortex. *Science* **350**, aac9462, doi:10.1126/science.aac9462 (2015).
- 852 70 Gerfen, C. R., Paletzki, R. & Heintz, N. GENSAT BAC cre-recombinase driver lines to study the
853 functional organization of cerebral cortical and basal ganglia circuits. *Neuron* **80**, 1368-1383,
854 doi:10.1016/j.neuron.2013.10.016 (2013).
- 855 71 Kolisnyk, B. *et al.* ChAT-ChR2-EYFP mice have enhanced motor endurance but show deficits in
856 attention and several additional cognitive domains. *The Journal of neuroscience : the official*
857 *journal of the Society for Neuroscience* **33**, 10427-10438, doi:10.1523/JNEUROSCI.0395-
858 13.2013 (2013).
- 859 72 Nakauchi, S., Brennan, R. J., Boulter, J. & Sumikawa, K. Nicotine gates long-term potentiation
860 in the hippocampal CA1 region via the activation of alpha2* nicotinic ACh receptors. *The*
861 *European journal of neuroscience* **25**, 2666-2681, doi:10.1111/j.1460-9568.2007.05513.x
862 (2007).
- 863 73 van Versendaal, D. *et al.* Elimination of inhibitory synapses is a major component of adult ocular
864 dominance plasticity. *Neuron* **74**, 374-383, doi:10.1016/j.neuron.2012.03.015 (2012).
- 865 74 Chen, J. L. *et al.* Clustered dynamics of inhibitory synapses and dendritic spines in the adult
866 neocortex. *Neuron* **74**, 361-373, doi:10.1016/j.neuron.2012.02.030 (2012).
- 867 75 Lazarus, M. S. & Huang, Z. J. Distinct maturation profiles of perisomatic and dendritic targeting
868 GABAergic interneurons in the mouse primary visual cortex during the critical period of ocular
869 dominance plasticity. *Journal of neurophysiology* **106**, 775-787, doi:10.1152/jn.00729.2010
870 (2011).
- 871 76 Wang, J. *et al.* An Accessory Agonist Binding Site Promotes Activation of alpha4beta2* Nicotinic
872 Acetylcholine Receptors. *The Journal of biological chemistry* **290**, 13907-13918,
873 doi:10.1074/jbc.M115.646786 (2015).
- 874 77 Wang, J. *et al.* A Novel alpha2/alpha4 Subtype-selective Positive Allosteric Modulator of
875 Nicotinic Acetylcholine Receptors Acting from the C-tail of an alpha Subunit. *The Journal of*
876 *biological chemistry* **290**, 28834-28846, doi:10.1074/jbc.M115.676551 (2015).
- 877 78 Timmermann, D. B. *et al.* Augmentation of cognitive function by NS9283, a stoichiometry-
878 dependent positive allosteric modulator of alpha2- and alpha4-containing nicotinic acetylcholine
879 receptors. *British journal of pharmacology* **167**, 164-182, doi:10.1111/j.1476-5381.2012.01989.x
880 (2012).
- 881 79 Reimers, K., Emmert, N., Shah, H., Benedict, R. H. & Szigeti, K. Capgras-like visual
882 decomposition in Lewy body dementia with therapeutic response to donepezil. *Neurology.*
883 *Clinical practice* **4**, 467-469, doi:10.1212/CPJ.0000000000000068 (2014).
- 884 80 Klassen, T. *et al.* Exome sequencing of ion channel genes reveals complex profiles confounding
885 personal risk assessment in epilepsy. *Cell* **145**, 1036-1048, doi:10.1016/j.cell.2011.05.025
886 (2011).

887 81 Conti, V. *et al.* Nocturnal frontal lobe epilepsy with paroxysmal arousals due to CHRNA2 loss of
888 function. *Neurology* **84**, 1520-1528, doi:10.1212/WNL.0000000000001471 (2015).

889 82 Yang, J. *et al.* The contribution of rare and common variants in 30 genes to risk nicotine
890 dependence. *Molecular psychiatry*, doi:10.1038/mp.2014.156 (2014).

891 83 Won, H. *et al.* Chromosome conformation elucidates regulatory relationships in developing
892 human brain. *Nature* **538**, 523-527, doi:10.1038/nature19847 (2016).

893 84 Tai, C., Abe, Y., Westenbroek, R. E., Scheuer, T. & Catterall, W. A. Impaired excitability of
894 somatostatin- and parvalbumin-expressing cortical interneurons in a mouse model of Dravet
895 syndrome. *Proceedings of the National Academy of Sciences of the United States of America*
896 **111**, E3139-3148, doi:10.1073/pnas.1411131111 (2014).

897 85 Paluszkiwicz, S. M., Olmos-Serrano, J. L., Corbin, J. G. & Huntsman, M. M. Impaired inhibitory
898 control of cortical synchronization in fragile X syndrome. *Journal of neurophysiology* **106**, 2264-
899 2272, doi:10.1152/jn.00421.2011 (2011).

900 86 Hashimoto, T. *et al.* Conserved regional patterns of GABA-related transcript expression in the
901 neocortex of subjects with schizophrenia. *The American journal of psychiatry* **165**, 479-489,
902 doi:10.1176/appi.ajp.2007.07081223 (2008).

903 87 Fung, S. J. *et al.* Expression of interneuron markers in the dorsolateral prefrontal cortex of the
904 developing human and in schizophrenia. *The American journal of psychiatry* **167**, 1479-1488,
905 doi:10.1176/appi.ajp.2010.09060784 (2010).

906 88 Lin, L. C. & Sibille, E. Reduced brain somatostatin in mood disorders: a common
907 pathophysiological substrate and drug target? *Frontiers in pharmacology* **4**, 110,
908 doi:10.3389/fphar.2013.00110 (2013).

909 89 Zhang, W. *et al.* Hyperactive somatostatin interneurons contribute to excitotoxicity in
910 neurodegenerative disorders. *Nature neuroscience* **19**, 557-559, doi:10.1038/nn.4257 (2016).

911 90 Schmid, L. C. *et al.* Dysfunction of Somatostatin-Positive Interneurons Associated with Memory
912 Deficits in an Alzheimer's Disease Model. *Neuron* **92**, 114-125,
913 doi:10.1016/j.neuron.2016.08.034 (2016).

914

Figure Legends

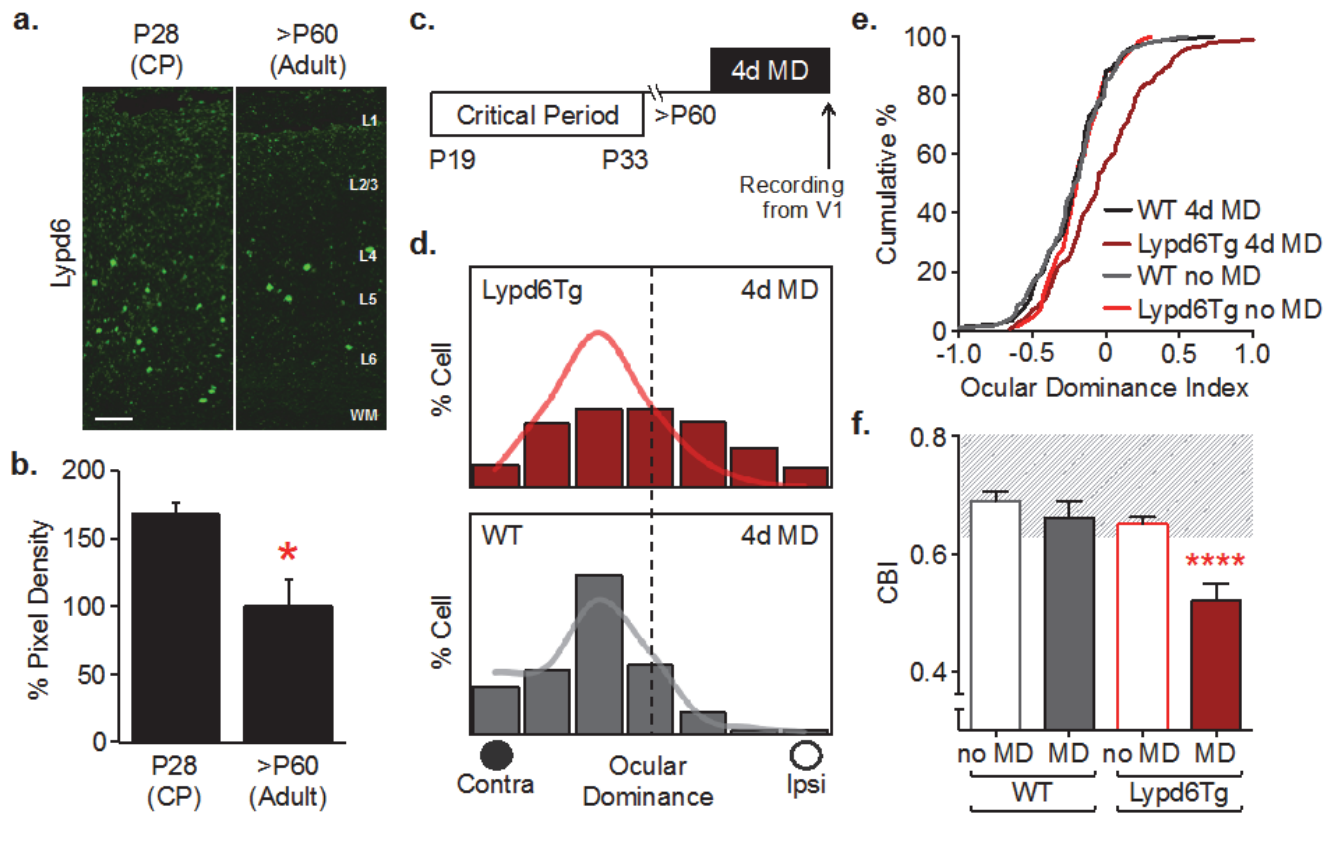


Figure 1 | Neuronal overexpression of Lypd6 prolongs ocular dominance plasticity into adulthood. (a) Representative images of fluorescent *in situ* hybridization labeling of *Lypd6* mRNA in V1 binocular zone from critical period (CP: P28) and adult (>P60) mice. Scale bar=100µm. (b) Quantification of *Lypd6* mRNA expression in V1 of P28 and >P60 mice. Data are mean±SEM of pixel intensity normalized to adult data. *Lypd6* level is higher in CP mice in comparison to Adult mice [CP: P28, n=4 mice; Adult: >P60, n=3 mice]: **P*=0.02, Student's *t*-test. Data are mean±SEM. (c) Schematic representation of V1 plasticity paradigm by 4 days of monocular deprivation (4d MD) in adult (>P60) *Lypd6Tg* or WT mice. (d) Adult 4d MD results in a shift in ocular dominance distribution of *Lypd6Tg* mice [red bar histogram; n=179 cells from 9 mice] but not in WT mice [gray bar histogram; n=86 cells from 7 mice]: *****P*<0.0001. *Lypd6Tg* 4d MD vs. *Lypd6Tg* no MD [red line histogram; n=67 cells from 4 mice]: *****P*<0.0001. *Lypd6Tg* no MD vs. WT no MD [gray line histogram; n=193 cells from 11 mice]:

$P=0.28$, χ^2 test. χ^2 tests were conducted based on actual cell numbers recorded. Histograms from groups for main comparisons are presented in bar format. Other control groups are overlaid in line format. Histograms are presented in percentage of cells representing each ocular dominance score. Filled circle labeled as “contra” represents contralateral eye that received monocular deprivation in MD designated groups, whereas empty circle labeled as “ipsi” represents the ipsilateral non-deprived eye. **(e)** Cumulative plot of quantified spike response of each unit (ocular dominance index) after adult 4d MD confirms ocular dominance shift in Lypd6Tg mice [red line; $n=179$ cells from 9 mice] but not in WT mice [black line; $n=86$ cells from 7 mice]: **** $P<0.0001$. Lypd6Tg 4d MD vs. Lypd6Tg no MD [bright red line; $n=67$ cells from 4 mice]: *** $P=0.0002$. Lypd6Tg no MD vs. WT no MD [gray line; $n=193$ cells from 11 mice]: $P=0.2332$, Kolmogorov-Smirnov (K-S) test. **(f)** Comparison of contralateral bias index (CBI) following adult 4d MD in WT mice [gray solid bar; CBI=0.66, $n=7$ mice] and Lypd6Tg mice [red solid bar; CBI=0.52, $n=9$ mice], or no MD in WT mice [gray open bar; CBI=0.66, $n=11$ mice] and Lypd6Tg mice [red open bar; CBI=0.65, $n=4$ mice]: **** $P<0.0001$, one-way analysis of variance (ANOVA). Lypd6Tg 4d MD significantly differs from all other groups: WT no MD, WT4d MD, and Lypd6Tg no MD: respectively, **** $P<0.0001$, ** $P=0.0023$, and * $P=0.0208$; Tukey’s multiple comparisons test. Gray background area represents CBI range in a non-plastic mouse. Data are mean \pm SEM.

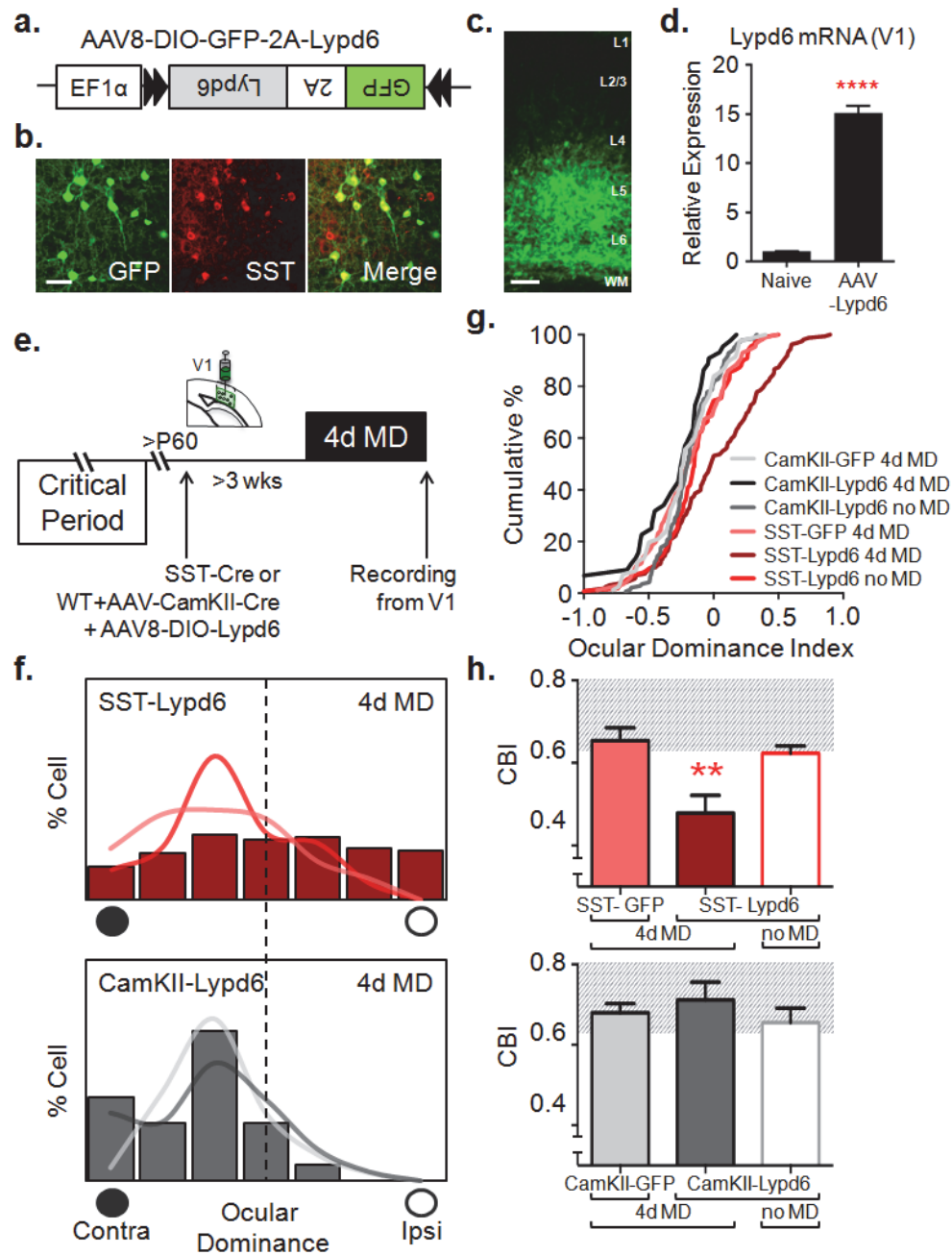


Figure 2 | Selective overexpression of Lypd6 specifically in SST interneurons reactivates ocular dominance plasticity in adult V1. (a) Schematic representation of adeno-associated viral (AAV) construct for cre-dependent Lypd6 over-expression. Bicistronic expression of GFP and Lypd6 is achieved through the use of a 2A sequence. (b) Representative images of viral GFP labeling following injection of AAV8-DIO-GFP-2A-Lypd6 (AAV-Lypd6) into V1 of SST-cre mice. Immunohistochemical

953 labeling shows specific expression of GFP (green) overlapping immunolabeled SST (red) neurons.
 954 $98 \pm 1.52\%$ of GFP labeled cells co-labeled with SST [$n=2$ mice]. Data are mean \pm SEM. Scale
 955 Bar=50 μ m. **(c)** Representative image of V1 layers following injection of AAV-Lypd6 targeting the deep
 956 layers in SST-Cre mice. Viral transduction represented by GFP (green) labeling is concentrated in
 957 layers V and VI. Scale Bar=100 μ m. **(d)** Quantitative PCR of *Lypd6* mRNA from cDNA derived from
 958 whole V1 extracts of naïve and AAV-Lypd6 injected SST-cre mice [$\Delta\Delta$ CT method, $n=3$ mice]:
 959 **** $P<0.0001$, Student's *t*-test. Data are mean \pm SEM. **(e)** Schematic representation of V1 plasticity
 960 paradigm by 4 days of monocular deprivation (4d MD) with viral injection. AAV-Lypd6 was injected into
 961 binocular zone of V1 of adult ($>P60$) SST-cre mice (SST-Lypd6), or as a cocktail with AAV-CamKII-cre
 962 in $>P60$ WT mice (CamKII-Lypd6) and incubated for >3 weeks prior to 4d MD. **(f)** Adult 4d MD results
 963 in a shift in ocular dominance distribution of SST-Lypd6 mice [red bar histogram; $n=158$ cells from 9
 964 mice] but not in WT mice injected with a cocktail of AAV-CamKII-cre and AAV-Lypd6 (CamKII-Lypd6)
 965 [gray bar histogram; $n=44$ cells from 3 mice]: **** $P<0.0001$. SST-Lypd6 4d MD: vs. SST-Lypd6 no MD
 966 [red line histogram; $n=110$ cells from 5 mice]: **** $P<0.0001$, vs. SST-GFP 4d MD [pink line histogram;
 967 $n=86$ cells from 5 mice]: *** $P=0.0006$. CamKII-Lypd6 4d MD vs. CamKII-GFP 4d MD [gray line
 968 histogram; $n=81$ cells from 4 mice]: $P=0.67$, χ^2 test. **(g)** Cumulative plot of ocular dominance index after
 969 adult 4d MD confirms ocular dominance shift in SST-Lypd6 mice [red line; $n=158$ cells from 9 mice] but
 970 not in CamKII-Lypd6 mice [black line; $n=44$ cells from 3 mice]: **** $P<0.0001$. SST-Lypd6 4d MD: vs.
 971 SST-Lypd6 no MD [bright red line; $n=110$ cells from 5 mice]: *** $P=0.0001$, vs. SST-GFP 4d MD [pink
 972 line; $n=86$ cells from 5 mice]: *** $P=0.0002$. CamKII-Lypd6 4d MD vs. CamKII-GFP 4d MD [light gray
 973 line; $n=81$ cells from 4 mice]: $P=0.49$, K-S test. **(h)** Comparison of contralateral bias index (CBI)
 974 following adult 4d MD in SST-GFP [pink solid bar; CBI=0.65, $n=5$ mice], SST-Lypd6 [red solid bar;
 975 CBI=0.48, $n=9$ mice], CamKII-GFP [light gray solid bar; CBI=0.68, $n=4$ mice] and CamKII-Lypd6 mice
 976 [dark gray solid bar; CBI=0.71, $n=3$ mice] with non-deprived SST-Lypd6 [red open bar; CBI=0.62, $n=5$
 977 mice] and non-deprived CamKII-Lypd6 [gray open bar; CBI=0.66, $n=5$ mice]: ** $P=0.0014$, one-way
 978 ANOVA. SST-Lypd6 4d MD significantly differs from: SST-Lypd6 no MD, SST-GFP 4d MD, and

979 CamKII-Lypd6 4d MD: respectively, $**P=0.0477$, $**P=0.0183$, and $***P=0.0073$. CamKII-Lypd6 4d MD
 980 does not differ from CamKII-Lypd6 no MD or CamKII-GFP 4d MD: respectively, $P=0.9527$, and
 981 $P=0.9969$; Tukey's multiple comparisons test. Gray background area represents CBI range in a non-
 982 plastic mouse. Data are mean \pm SEM.
 983

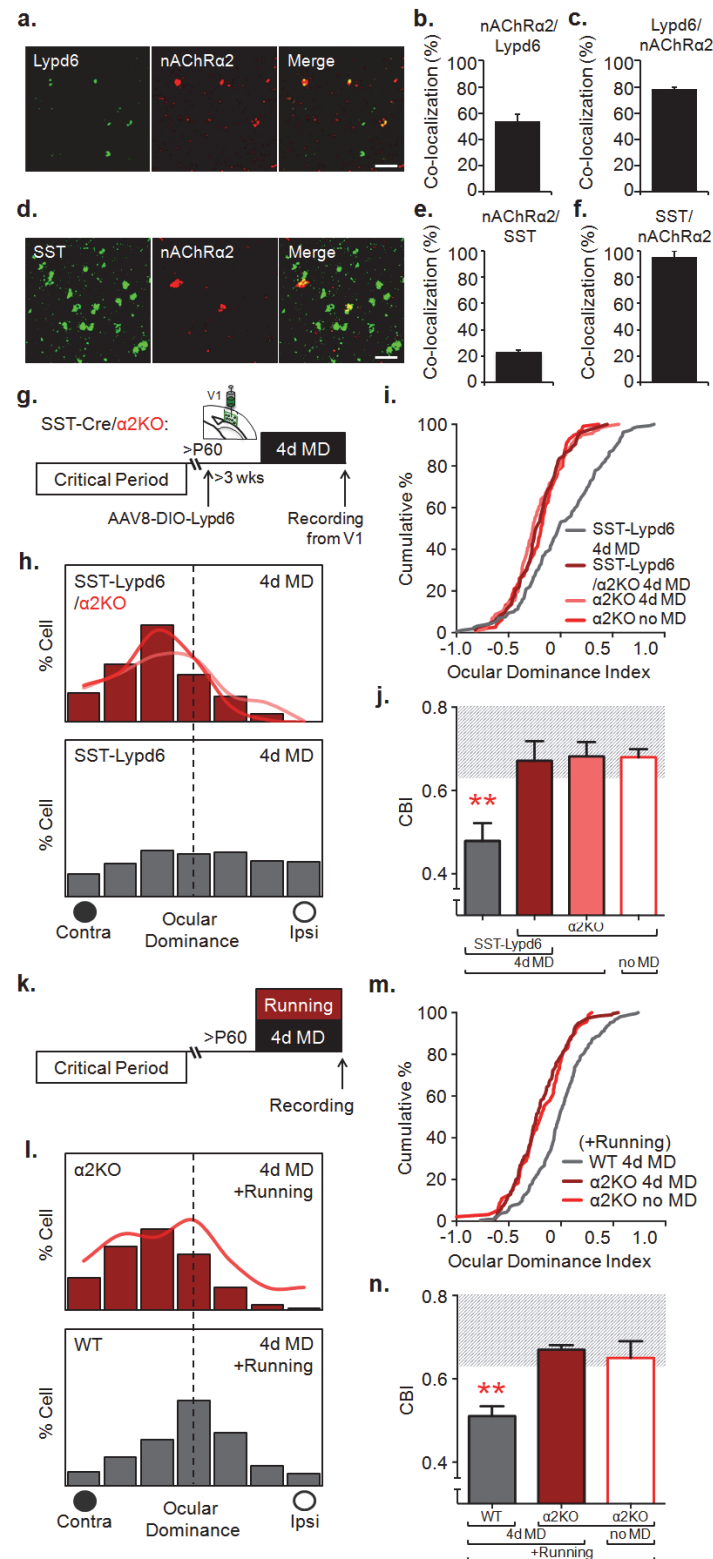


Figure 3 | $\alpha 2$ nicotinic acetylcholine receptor subunit is required for reactivation of ocular dominance plasticity in adulthood. (a) Representative images of double fluorescent *in situ*

987 hybridization labeling of mRNA in V1 for *Lypd6* (green) and $\alpha 2$ *nicotinic acetylcholine receptor*
988 (*nAChRa2*) (red). Scale bar=50 μ m. **(b)** 53 \pm 3.26% of *Lypd6* mRNA labeled cells co-express *nAChRa2*
989 mRNA. [n=2 mice]. **(c)** 79 \pm 2.93% of *nAChRa2* mRNA labeled cell co-express *Lypd6* mRNA. [n=2 mice].
990 Data are mean \pm SEM. **(d)** Representative images of double fluorescent *in situ* hybridization labeling of
991 mRNA in V1 for *SST* (green) and $\alpha 2$ *nicotinic acetylcholine receptor* (*nAChRa2*) (red). Scale bar=50 μ m.
992 **(e)** 23 \pm 0.01% of *SST* mRNA labeled cell co-express *nAChRa2* mRNA. [n= 2 mice]. **(f)** 95 \pm 0.04% of
993 *nAChRa2* mRNA labeled cells co-express *SST* mRNA. [n=2 mice]. Data are mean \pm SEM. **(g)**
994 Schematic representation of experiment for **h-j**; V1 plasticity paradigm by 4 days of monocular
995 deprivation (4d MD) with viral injection. AAV-*Lypd6* was injected into V1 binocular zone of adult (>P60)
996 bigenic *SST-cre/Chrna2KO* mice (*SST-Lypd6/α2KO*), or >P60 *SST-cre* mice (*SST-Lypd6*) and
997 incubated for >3 weeks prior to 4d MD. **(h)** Adult 4d MD results in a significantly decreased shift in
998 ocular dominance distribution of bigenic *SST-Lypd6/α2KO* mice [red bar histogram; n=73 cells from 5
999 mice] when compared with ocular dominance shift in adult 4d MD *SST-Lypd6* mice [gray bar histogram;
1000 data in Fig. 2e legend]: **** P <0.0001. *SST-Lypd6/α2KO* 4d MD vs. $\alpha 2$ KO 4d MD [pink line histogram;
1001 n=116 cells from 3 mice]: P =0.62. $\alpha 2$ KO 4d MD vs. $\alpha 2$ KO no MD [red line histogram; n=114 cells from
1002 4 mice]: P =0.24, χ^2 test. **(i)** Cumulative plot of ocular dominance index after adult 4d MD confirms
1003 significant ablation of ocular dominance shift in absence of *nAChRa2* in deprived *SST-Lypd6/α2KO*
1004 mice [red line; n=73 cells from 5 mice] compared with *SST-Lypd6* mice [gray line; data in Fig. 2f
1005 legend]: **** P <0.0001. *SST-Lypd6/α2KO* 4d MD vs. $\alpha 2$ KO 4d MD [pink line; n=116 cells from 3 mice]:
1006 P =0.64. $\alpha 2$ KO 4d MD vs. $\alpha 2$ KO no MD [bright red line; n=114 cells from 4 mice]: P =0.06, K-S test. **(j)**
1007 Comparison of contralateral bias index (CBI) following adult 4d MD in *SST-Lypd6* mice [gray solid bar;
1008 data in Fig. 2g legend], *SST-Lypd6/α2KO* mice [red solid bar; CBI=0.66, n=5 mice], and $\alpha 2$ KO mice
1009 [pink solid bar; CBI=0.68, n=3 mice], or no MD in $\alpha 2$ KO mice [bright red open bar; CBI=0.68, n=4 mice]:
1010 ** P =0.0053, one-way ANOVA. *SST-Lypd6/α2KO* 4d MD is only significantly different with *SST-Lypd6*
1011 4d MD: * P =0.0209, and is not different from $\alpha 2$ KO 4d MD: P =0.9990. $\alpha 2$ KO 4d MD vs. $\alpha 2$ KO no MD:
1012 P >0.9999; Tukey's multiple comparisons test. Gray background area represents CBI range in a non-

1013 plastic mouse. Data are mean±SEM. **(k)** Schematic representation of experiment for **I-n**; V1 plasticity
1014 paradigm by 4 days of monocular deprivation (4d MD) with simultaneous 4 days of voluntary physical
1015 exercise through the use of a running wheel (Running) in single housed adult (>P60) Chrna2KO and
1016 WT mice. **(l)** Adult 4d MD with simultaneous Running results in a shift in ocular dominance distribution
1017 of WT mice [gray bar histogram; n=207 cells from 5 mice] but not in Chrna2KO mice [red bar
1018 histogram; n=194 cells from 4 mice]: **** $P<0.0001$, χ^2 test. Chrna2KO 4d MD +Running vs Chrna2KO
1019 no MD+ Running [red line histogram; n=93 cells from 4 mice]: $P=0.35$, χ^2 test. **(m)** Cumulative plot of
1020 ocular dominance index after adult 4d MD with simultaneous Running confirms ocular dominance shift
1021 in WT mice [gray line; n=207 cells from 5 mice] but not in Chrna2KO mice [red line; n=194 cells from 4
1022 mice]: **** $P<0.0001$. Chrna2KO 4d MD+Running vs. Chrna2KO no MD+Running: $P=0.33$, K-S test. **(n)**
1023 Comparison of contralateral bias index (CBI) following adult 4d MD with simultaneous Running in WT
1024 mice [gray solid bar; CBI=0.51, n=5 mice] and Chrna2KO mice [red solid bar; CBI=0.67, n=4 mice], or
1025 no MD with simultaneous Running in Chrna2KO mice [red open bar; CBI=0.65, n=4 mice]: ** $P=0.0030$,
1026 one-way ANOVA. Chrna2KO 4d MD+Running vs WT 4d MD+Running: ** $P=0.0046$, vs Chrna2KO no
1027 MD+Running: ** $P=0.0103$; Tukey's multiple comparisons test. Gray background area represents CBI
1028 range in a non-plastic mouse. Data are mean±SEM.

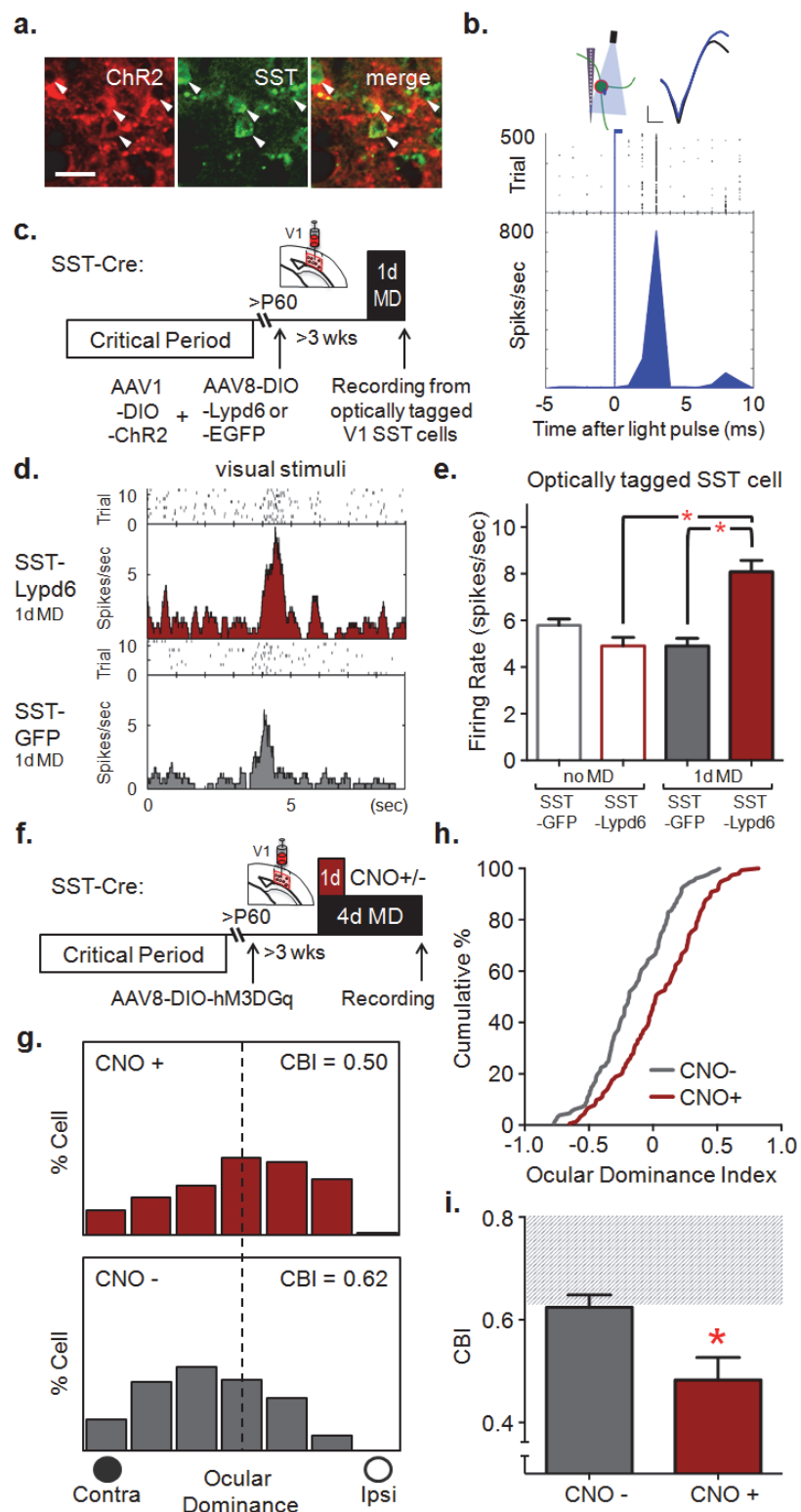


Figure 4 | Lypd6 in SST interneurons increase SST interneuron activity to express ocular dominance plasticity. (a) Representative images of viral mCherry labeling following injection of AAV-

1032 DIO-hChR2 (AAV-ChR2) into the V1 of SST-cre mice. ChR2/mCherry (red) is specifically expressed in
1033 immunolabeled SST (green) neuron. $95 \pm 1.86\%$ of mCherry labeled cells co-labeled with SST. [n=2
1034 mice]. Data are mean \pm SEM. Scale bar=25 μ m. **(b)** Example of an optically-tagged SST interneuron
1035 showing time locked optogenetic activation. Laser (wavelength 473 nm, fiber diameter 105 μ m) was
1036 delivered using an optic fiber coupled to the multichannel extracellular recording electrode. The fiber tip
1037 was positioned immediately above the V1 recording site. SST+ cells were identified with a light pulse
1038 (1ms, 20Hz) stimulus. **(c)** Schematic representation of experiments in **d-e**. Adult (>P60) SST-cre mice
1039 were injected with a combination of AAV-ChR2 and either AAV-Lypd6 (SST-Lypd6) or AAV-EGFP
1040 (SST-GFP) into V1 binocular zone and incubated for >3 weeks prior to 1 day of monocular deprivation
1041 (1d MD), after which extracellular recordings were conducted to collect and analyze visually evoked
1042 firing rates of optically-tagged SST interneurons. **(d)** Representative histograms of visually evoked firing
1043 of optically-tagged SST interneurons after adult 1d MD in SST-Lypd6 [top, red] and SST-GFP [gray,
1044 bottom]. **(e)** Comparison of visually evoked firing rate following adult 1d MD in SST-GFP [gray solid bar;
1045 n=68 cells, 4 mice] and SST-Lypd6 [red solid bar; n=101 cells, 5 mice] with non-deprived (no MD) SST-
1046 GFP [gray open bar; n=82 cells, 5 mice] and SST-Lypd6 [red open bar; n=38 cells, 3 mice]. Data are
1047 mean \pm SEM. Overexpression of Lypd6 results in a significant increase in visually evoked firing rate of
1048 SST interneurons after 1d MD (SST-Lypd6 1d MD) in comparison to SST-GFP 1d MD and SST-Lypd6
1049 no MD (respectively, $*P=0.0137$ and $*P=0.0339$, *Linear Mixed Model (LMM)* – animal considered as
1050 random effect, genetic manipulation (-GFP or -Lypd6) and experience (1d MD or no MD) considered as
1051 fixed effects; multiple comparisons corrected by Tukey's method). **(f)** Schematic representation of V1
1052 plasticity paradigm by 4 days of monocular deprivation (4d MD) with viral injection. AAV8-DIO-
1053 hM4D(Gq)-mCherry (AAV8-GqDREADD) was injected into V1 binocular zone of adult (>P60) SST-cre
1054 mice and incubated for >3 weeks prior to 4d MD. CNO (CNO+) or saline (CNO-) was given during the
1055 first day of 4d MD to chemogenetically activate viral GqDREADD expressing SST interneurons for only
1056 1 day. Following 4d MD, extracellular recordings were performed for analysis of ocular dominance. **(g)**
1057 Chemogenetic activation of SST interneurons during the first day of 4d MD through CNO delivery

1058 [CNO+: red, n=154 cells from 5 mice] results in a significant shift in ocular dominance distribution, but
 1059 not when given saline [CNO-: gray, n=129 cells from 5 mice]: *** $P=0.0007$, χ^2 test. **(h)** Cumulative plot
 1060 of ocular dominance index after adult 4d MD confirms ocular dominance shift after 1 day-activation of
 1061 SST interneurons in CNO+ mice [red line, n=154 cells from 5 mice] compared with CNO- [gray line,
 1062 n=129 cells from 5 mice]: ** $P<0.0001$, K-S test. **(i)** Comparison of contralateral bias index (CBI)
 1063 following 4d MD in SST-cre mice injected with AAV-GqDREADD and administered either CNO [CNO+:
 1064 red solid bar, CBI=0.50; n=5 mice] or saline [CNO-: gray solid bar, CBI=0.62; n=5 mice] during the first
 1065 day of 4d MD: * $P=0.0208$, Student's *t*-test. Gray background area represents CBI range in a non-plastic
 1066 mouse. Data are mean \pm SEM.

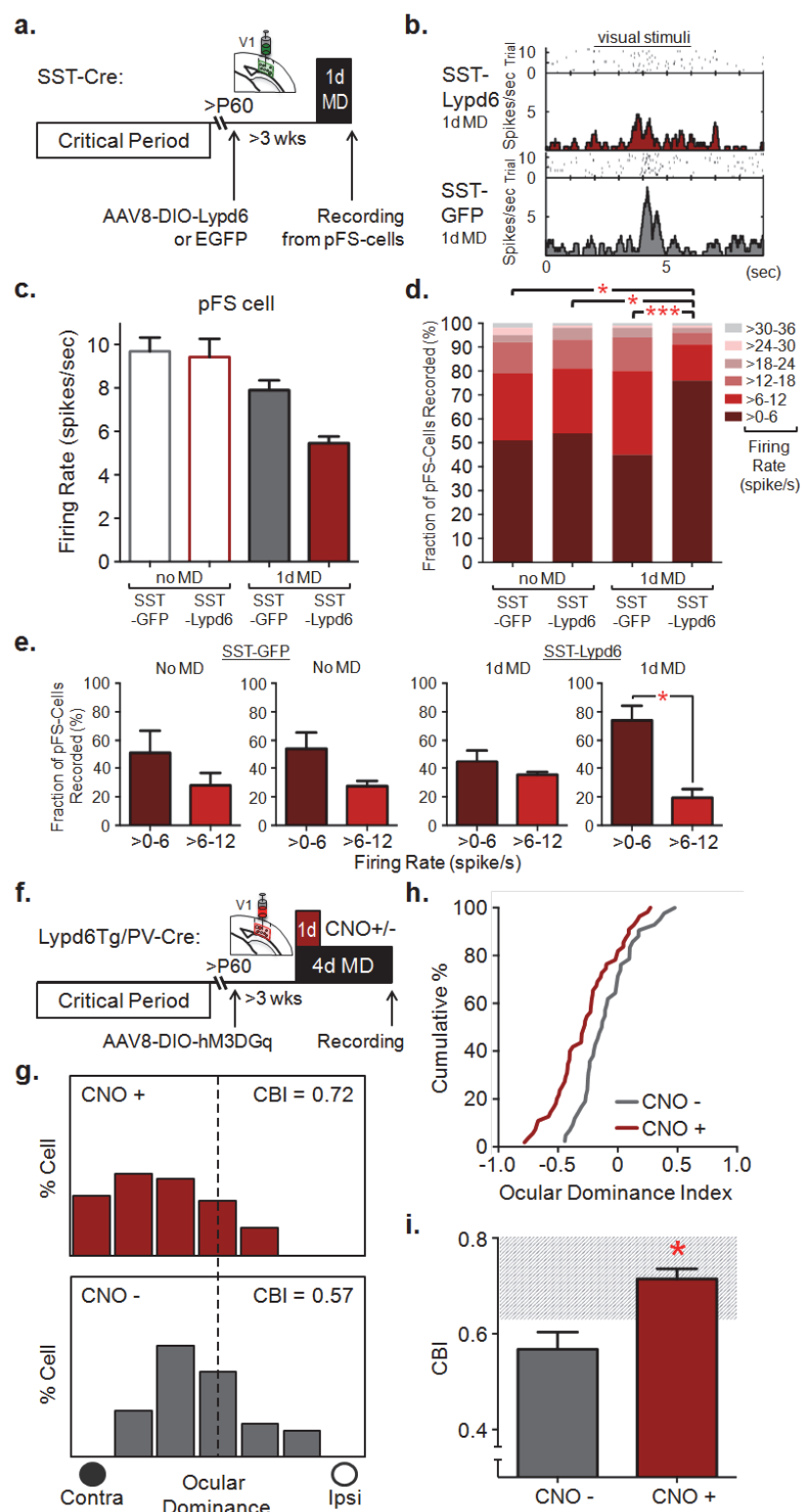
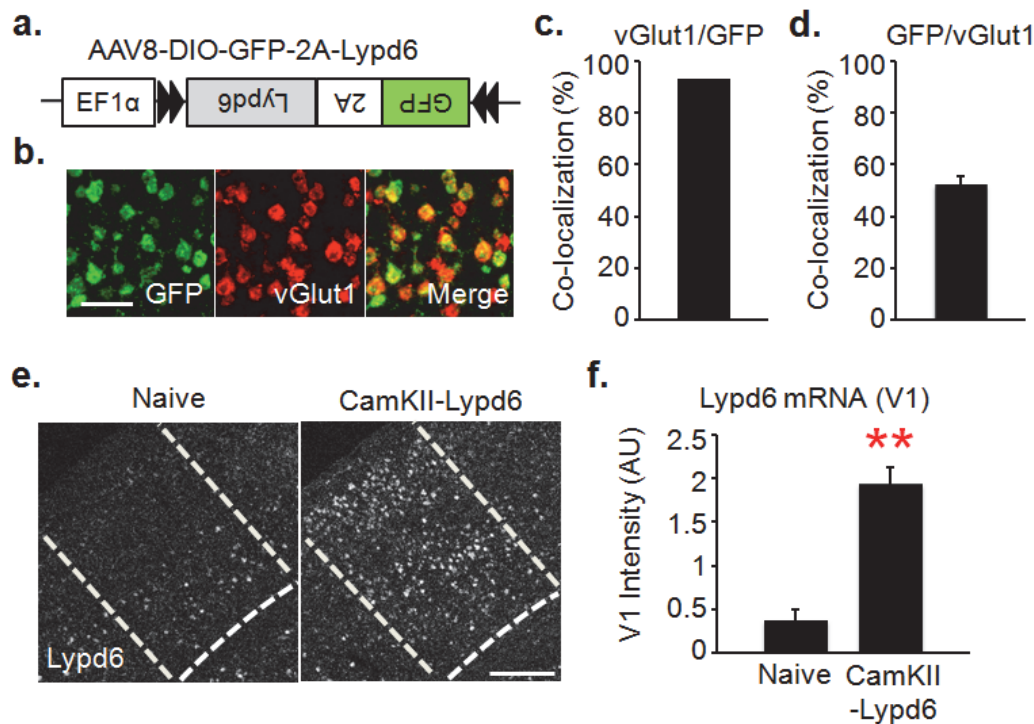


Figure 5 | Lypd6 in SST interneurons suppress PV interneuron activity to express ocular dominance plasticity. (a) Schematic representation of experiments in b-c. Adult (>P60) SST-cre mice

were injected with AAV-Lypd6 (SST-Lypd6) or AAV-EGFP (SST-GFP) into V1 binocular zone and incubated for >3 weeks prior to 1 day of monocular deprivation (1d MD), after which extracellular recordings were conducted to collect and analyze visually evoked firing rates of putative fast-spiking (pFS) cells sorted by their narrow spike width. For sorting details see *Methods* and *Supplemental Figure 2*. (b) Representative histograms of visually evoked firing of pFS cells after adult 1d MD in SST-Lypd6 [top, red] and SST-GFP [gray, bottom]. (c) Comparison of cell-level means of visually evoked firing rate using standard binomial tests show significant decrease in visually evoked firing rate of pFS cells in SST-Lypd6 1d MD [red solid bar; n=170 cells, 7 mice], in comparison to all other groups: SST-GFP 1d MD [gray solid bar; n=148 cells, 5 mice], SST-Lypd6 no MD [red open bar; n=63 cells, 4 mice], and SST-GFP no MD [gray open bar; n=116 cells, 5 mice]: **** $P < 0.0001$, one-way analysis of variance (ANOVA). Significance for each comparisons are respectively, *** $P = 0.0007$, **** $P < 0.0001$, and **** $P < 0.0001$; Bonferroni's multiple comparisons test. When fitted to a *Linear Mixed Model (LMM)*, SST-Lypd6 1d MD group shows a trending reduction with no statistical significance in comparison to all other groups, confirmed by pairwise tests with SST-GFP 1d MD, SST-Lypd6 no MD, and SST-GFP no MD (respectively, $P = 0.211$, $P = 0.2301$, and $P = 0.1161$ – animal considered as random effect, genetic manipulation (-GFP or -Lypd6) and experience (1d MD or no MD) considered as fixed effects; multiple comparisons corrected by Tukey's method). All other comparisons under LMM between SST-Lypd6 no MD, SST-GFP no MD, and SST-GFP 1d MD have $P > 0.98$. Data are mean \pm SEM. (d) Frequency distributions of firing rates in putative PV (pFS) interneurons, sorted by their narrow spike width, in adult (>P60) mice. The firing rates across all groups were separated into 6 bins of 6 spikes/second. A significantly higher distribution of visually evoked firing rates towards the lowest bin shows 1d MD results in a decrease in visually evoked firing rate of pFS cells only when Lypd6 is overexpressed in adult SST interneurons [SST-Lypd6 1d MD; n=7 mice, 170 cells] in comparison to non-Lypd6 overexpressing (SST-GFP) or non-deprived (no MD) groups: [SST-GFP 1d MD; n=5 mice, 148 cells]: *** $P = 0.0009$, [SST-Lypd6 no MD; n=4 mice 63 cells]: * $P = 0.0454$, [SST-GFP no MD; n=5 mice, 116 cells]: * $P = 0.0160$, χ^2 tests were conducted based on actual cell numbers recorded. (e) Adult SST-cre

1096 mice overexpressing Lypd6 after 1d MD [SST-Lypd6 1d MD; n=7 mice] but no other groups [SST-GFP
1097 1d MD, n=5 mice; SST-Lypd6 no MD, n=4 mice; SST-GFP no MD, n=5 mice] have significantly higher
1098 fraction of pFS interneuron firing rate in the lowest bin (>0-6) in comparison to the bin above (>6-12):
1099 $*P=0.0136$, Student's *t*-test. Data are mean \pm SEM. **(f)** Schematic representation of V1 plasticity
1100 paradigm by 4 days of monocular deprivation (4d MD) with viral injection. AAV8-GqDREADD was
1101 injected into V1 binocular zone of adult (>P60) bigenic Lypd6Tg/PV-cre mice and incubated for >3
1102 weeks prior to 4d MD. CNO (CNO+) or saline (CNO-) was given during the first day of 4d MD to
1103 chemogenetically activate viral GqDREADD expressing PV interneurons for only 1 day. Following 4d
1104 MD, extracellular recordings were performed for analysis of ocular dominance. **(g)** Chemogenetic
1105 activation of PV interneurons during the first day of 4d MD through CNO delivery [CNO+: red, n=55
1106 cells from 4 mice] results in a significant decrease in ocular dominance shift, but not when given saline
1107 [CNO-: gray, n=42 cells from 3 mice]: $**P=0.0030$, χ^2 test. **(h)** Cumulative plot of ocular dominance
1108 index after adult 4d MD confirms decreased ocular dominance shift after 1 day-activation of PV
1109 interneurons in CNO+ mice [red line, n=55 cells from 4 mice] compared with CNO- [gray line, n=42
1110 cells from 3 mice]: $**P=0.0054$, K-S test. (i) Comparison of contralateral bias index (CBI) following 4d
1111 MD in SST-cre mice injected with AAV-GqDREADD and administered either CNO [CNO+: red solid
1112 bar, CBI=0.71; n=4 mice] or saline [CNO-: gray solid bar, CBI=0.57; n=3 mice] during the first day of 4d
1113 MD: $*P=0.0128$, Student's *t*-test. Gray background area represents CBI range in a non-plastic mouse.
1114 Data are mean \pm SEM.

Supplementary Information

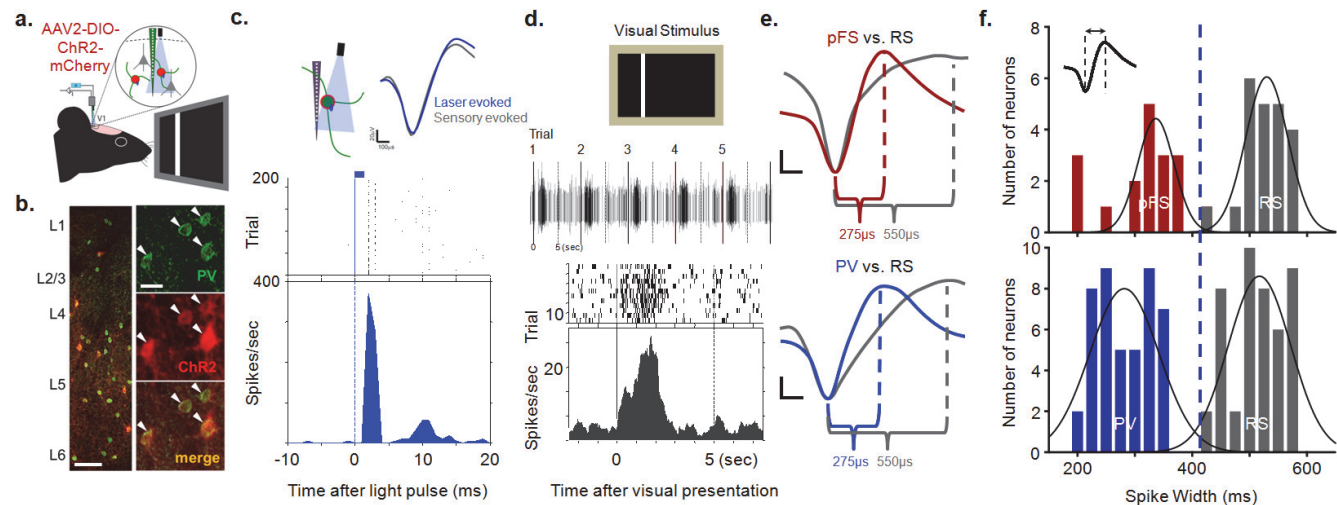


1116

Supplementary Figure 1 | Validation of over-expression of Lypd6 in glutamatergic V1 neurons.

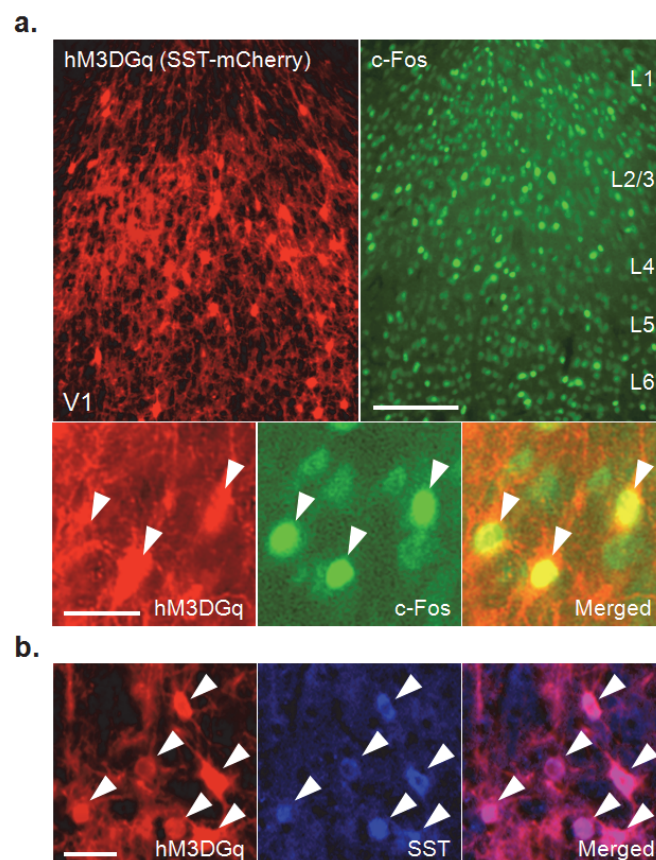
(a) Schematic representation of adeno-associated viral Cre-dependent Lypd6 over-expression construct. (b) Representative double *in situ* hybridization labeling of viral GFP following a cocktail injection of AAV-DIO-GFP-Lypd6 and AAV-CamKII-Cre into V1 binocular zone shows specific expression of GFP (green) in vGlut1 (red)-positive neurons. Scale bar=50μm. (c) 93.2±1.6% of viral GFP positive cells co-express vGlut1. [n=3 mice]. Data are mean±SEM. (d) 52.2±3% of vGlut1 positive cells co-express viral GFP. [n=3 mice]. Data are mean±SEM. (e) Representative images of fluorescent *in situ* hybridization labeling of Lypd6 in V1 binocular zone from the non-injected control hemisphere (naive) and the virus cocktail injected hemisphere (CamKII-Lypd6). V1 Binocular zone is outlined by dashed white-line, based on Paxinos and Franklin's The Mouse Brain in Stereotaxic Coordinates (1997). Scale bar=200μm. (f) Quantification of Lypd6 expression in V1 binocular zone from the CamKII-Lypd6 and naïve hemispheres. Absolute intensity for every Lypd6 positive cells in the binocular V1 was summed and the total value was subsequently divided by the μm² area of images of V1 binocular zone.

1130 Lypd6 expression is significantly higher in the CamKII-Lypd6 hemisphere in comparison to the naïve
 1131 hemisphere [5 sections from 2 mice] $P=0.0049$, Student's t -test for paired samples. Data are
 1132 mean \pm SEM.

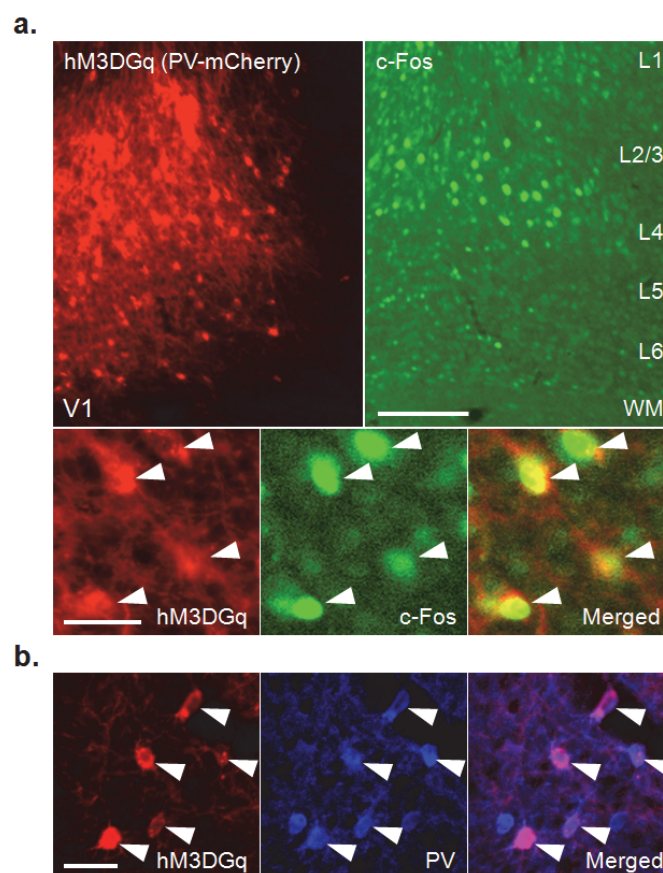


Supplementary Figure 2 | Defining putative fast-spiking (pFS) cells based on optogenetic tagging of PV interneuron. pFS cells were defined by a criteria established from the spike width of optogenetically tagged PV interneurons. **(a-c)** Optogenetic tagging of PV interneurons. **(a)** Schematic representation of expression of adeno-associated viral Cre-dependent ChR2 expression construct (AAV-DIO-ChR2-mCherry) in PV interneurons of V1 binocular zone of PV-cre mice. **(b)** Representative images of robust viral mCherry labeling following injection of AAV-DIO-ChR2 into V1 binocular zone of PV-cre mice. Immunohistochemical labeling shows specific expression of ChR2/mCherry (red) in immunolabeled PV (green) interneurons. Left inset scale bar=100 μ m, right insets scale bar=25 μ m. **(c)** Example of optogenetically tagged PV interneuron showing time locked optogenetic activation. Laser (wavelength 473 nm, fiber diameter 105 μ m) was delivered using an optic fiber coupled to the 16-channel linear silicone probe. The fiber tip was positioned immediately above the recording site. PV+ cells were identified with a light pulse (1msec, 1Hz) stimulus. **(d)** Example of visually evoked responses from a putative PV interneuron (putative fast spiking: pFS cell, in e and f) identified and sorted through optogenetic tagging method in c. Top trace represents a series of a single pFS cell's visually evoked responses after 5 consecutive trials of visual stimulus presentation (solid black line represents onset of visual stimulus and dotted line represents termination of visual stimulus). The middle raster plot represents the responses of the single pFS cell across all 12 trials. Bottom histogram is a result of

1151 peristimulus analysis of peak to baseline spike activity in response to the visual stimulus (solid line
 1152 represents onset of visual stimulus and dotted line represents termination of visual stimulus). **(e)** The
 1153 method for properly identifying PV interneurons without optogenetic tagging was based on a spike-
 1154 width-based criterion based on responses of optogenetically identified PV interneurons. Top: An
 1155 averaged visually evoked spike waveform of putative fast spiking (pFS, red) overlaid on a regular
 1156 spiking cell (RS, gray) waveform. Bottom: An averaged visually evoked spike waveform of
 1157 optogenetically-tagged PV+ cell (PV, blue) overlaid on a regular spiking cell (RS, gray) waveform.
 1158 Scale represents x:100ms, y: 20mV. Both pFS and PV waveforms have identical spike width duration
 1159 ($275 \mu s$) in comparison to average RS waveform spike width duration ($550 \mu s$). **(f)** A population of
 1160 pFS cells [red: 16 cells, 3 mice] were defined as the neurons whose spike-width (trough-to-peak time) is
 1161 under 412ms (blue line), which was based on the spike-width of optically tagged PV interneuron
 1162 recording [blue: 45 cells, 3 mice]. Firing rates of pFS cells are comparable to those of optically tagged
 1163 PV interneurons.
 1164



Supplementary Figure 3 | Validation of AAV-GqDREADD expression and chemogenetic activation of SST interneurons. (a) Representative of c-fos activation (green) of AAV-GqDREADD infected SST interneurons. Scale bar=200µm. SST-cre mice virally injected with AAV8-GqDREADD in V1 binocular zone were perfused 90 minutes after CNO injection (0.6 mg/kg) to capture the neural activation. Note c-fos-positive cells (green) are restricted to the area where mCherry-positive cells (red) are clustered. Scale bar=50µm. (b) Representative images of viral mCherry labeling following injection of AAV-GqDREADD into V1 of SST-cre mice. Immunohistochemical labeling shows specific expression of GqDREADD/mCherry (red) in immunolabeled SST (blue) neurons. Scale bar=50µm.



Supplementary Figure 4 | Validation of AAV-GqDREADD expression and chemogenetic activation of PV interneurons. (a) Representative of c-fos activation (green) of AAV-GqDREADD infected PV interneurons. Scale bar=200µm. PV-cre mice virally injected with AAV8-GqDREADD in V1 binocular zone were perfused 90 minutes after CNO injection (0.6 mg/kg) to capture the neural activation. Note c-fos-positive cells (green) are restricted to the area where mCherry-positive cells (red) are clustered. Scale bar=50µm. (b) Representative images of viral mCherry labeling following injection of AAV-GqDREADD into V1 of PV-cre mice. Immunohistochemical labeling shows specific expression of GqDREADD/mCherry (red) in immunolabeled PV (blue) neurons. Scale bar=50µm.